OPEN ACCESS

ORIGINAL ARTICLE

Liver PPARα is crucial for whole-body fatty acid homeostasis and is protective against NAFLD

Alexandra Montagner,[1] Arnaud Polizzi,[1] Edwin Fouché,[1] Simon Ducheix,[1] Yannick Lippi,[1] Frédéric Lasserre,[1] Valentin Barquissau,[2,3] Marion Régnier,[1] Céline Lukowicz,[1] Fadila Benhamed,[4,5,6] Alison Iroz,[4,5,6] Justine Bertrand-Michel,[2,3] Talal Al Saati,[7] Patricia Cano,[1] Laila Mselli-Lakhal,[1] Gilles Mithieux,[8] Fabienne Rajas,[8] Sandrine Lagarrigue,[9,10,11] Thierry Pineau,[1] Nicolas Loiseau,[1] Catherine Postic,[4,5,6] Dominique Langin,[2,3,12] Walter Wahli,[1,13,14] Hervé Guillou[1]

▶ Additional material is published online only. To view please visit the journal online (http://dx.doi.org/10.1136/gutjnl-2015-310798).

For numbered affiliations see end of article.

Correspondence to
Dr Hervé Guillou, INRA UMR1331, ToxAlim, Chemin de Tournefeuille, Toulouse 31027, France; herve.guillou@toulouse.inra.fr
or
Prof. Walter Wahli Lee Kong Chian School of Medicine Nanyang Technological University The Academia, 20 College Road, Singapore 169856; walter.wahli@ntu.edu.sg

Received 25 September 2015
Revised 28 December 2015
Accepted 4 January 2016
Published Online First 2 February 2016

Open Access
Scan to access more free content

Linked

▶ http://dx.doi.org/10.1136/gutjnl-2016-311408

CrossMark

To cite: Montagner A, Polizzi A, Fouché E, *et al*. *Gut* 2016;**65**:1202–1214.

ABSTRACT

Objective Peroxisome proliferator-activated receptor α (PPARα) is a nuclear receptor expressed in tissues with high oxidative activity that plays a central role in metabolism. In this work, we investigated the effect of hepatocyte PPARα on non-alcoholic fatty liver disease (NAFLD).

Design We constructed a novel hepatocyte-specific PPARα knockout (*Pparα*$^{hep-/-}$) mouse model. Using this novel model, we performed transcriptomic analysis following fenofibrate treatment. Next, we investigated which physiological challenges impact on PPARα. Moreover, we measured the contribution of hepatocytic PPARα activity to whole-body metabolism and fibroblast growth factor 21 production during fasting. Finally, we determined the influence of hepatocyte-specific PPARα deficiency in different models of steatosis and during ageing.

Results Hepatocyte PPARα deletion impaired fatty acid catabolism, resulting in hepatic lipid accumulation during fasting and in two preclinical models of steatosis. Fasting mice showed acute PPARα-dependent hepatocyte activity during early night, with correspondingly increased circulating free fatty acids, which could be further stimulated by adipocyte lipolysis. Fasting led to mild hypoglycaemia and hypothermia in *Pparα*$^{hep-/-}$ mice when compared with *Pparα*$^{-/-}$ mice implying a role of PPARα activity in non-hepatic tissues. In agreement with this observation, *Pparα*$^{-/-}$ mice became overweight during ageing while *Pparα*$^{hep-/-}$ remained lean. However, like *Pparα*$^{-/-}$ mice, *Pparα*$^{hep-/-}$ fed a standard diet developed hepatic steatosis in ageing.

Conclusions Altogether, these findings underscore the potential of hepatocyte PPARα as a drug target for NAFLD.

Significance of this study

What is already known on this subject?

- Peroxisome proliferator-activated receptor α (PPARα) is a nuclear receptor expressed in many tissues and is responsible for several important metabolic controls, especially during fasting.
- PPARα is a target for the hypolipidemic drugs of the fibrate family.
- PPARα is less expressed in the liver of patients with non-alcoholic fatty liver diseases (NAFLD).
- Several PPAR-targeting molecules, including dual agonists, are currently under investigation for NAFLD treatment.

What are the new findings?

- Hepatocyte-restricted PPARα deletion impairs liver and whole-body fatty acid homeostasis.
- Hepatic PPARα responds to acute and chronic adipose tissue lipolysis.
- Hepatic PPARα regulates circadian fibroblast growth factor 21 (FGF21) and fasting-induced FGF21, and is partially responsible for the FGF21 increase in steatohepatitis.
- Hepatocyte-restricted PPARα deletion is sufficient to promote NAFLD and hypercholesterolaemia during ageing, but does not lead mice to become overweight.

How might it impact on clinical practice in the foreseeable future?

- This work emphasises the relevance and potential of hepatic PPARα as a drug target for NAFLD.

INTRODUCTION

Precise control of fatty acid metabolism is essential. Defective fatty acid homeostasis regulation may induce lipotoxic tissue damage, including hepatic steatosis.[1] Peroxisome proliferator-activated receptors (PPARs) are transcription factors that serve as fatty acid receptors and help regulate gene expression in response to fatty acid-derived stimuli.[2] PPARs act as ligand-activated receptors, controlling target gene transcription. The three PPAR isotypes, PPARα, PPARβ/δ and PPARγ, display specific tissue expression patterns and control different biological functions,[3] but all bind lipids and control lipid homeostasis in different tissues, including the liver.[2]

A healthy liver does not accumulate lipids, but it plays central roles in fatty acid anabolism and export to peripheral organs, including white

adipose tissue for energy storage.[4] During dietary restriction, hepatic fatty acid catabolism is also critical for using free fatty acids (FFAs) released from white adipose tissues. PPARα is the most abundant isotype in hepatocytes and is involved in many aspects of lipid metabolism,[5 6] including fatty acid degradation, synthesis, transport, storage, lipoprotein metabolism and ketogenesis during fasting.[7–9] In addition, PPARα controls glycerol use for gluconeogenesis[9] as well as autophagy[10] in response to fasting. Moreover, PPARα regulates the expression of the fibroblast growth factor 21 (FGF21) during starvation.[11 12] In turn, FGF21 acts as an endocrine hormone targeting various functions including metabolic control.[13] Finally, PPARα helps repress the acute-phase response and inflammation in the liver.[14]

Obesity can lead to organ and vascular complications.[15] Non-alcoholic fatty liver disease (NAFLD), which are considered the hepatic manifestation of metabolic syndrome, range from benign steatosis to severe non-alcoholic steatohepatitis (NASH), potentially further damaging organs.[16] Sustained elevation of neutral lipid accumulation (mostly triglycerides in hepatocyte lipid droplets) initiates early pathological stages. Different fatty acid sources contribute to fatty liver development, including dietary lipid intake, de novo lipogenesis and adipose tissue lipolysis.[4] In NAFLD, 60% of fatty acids accumulated in steatotic liver are adipose-derived.[17]

Preclinical[18–21] and clinical[22] studies highlight that PPARα influences NAFLD and NASH. Mice lacking PPARα develop steatosis during fasting,[7 8] suggesting the importance of PPARα activity for using FFA released from adipocytes. However, PPARα is expressed and active in many tissues, including skeletal muscles,[23] adipose tissues,[24 25] intestines,[26] kidneys[27] and heart,[28] which all contribute to fatty acid homeostasis. Therefore, it remains unknown whether the increased steatosis susceptibility in mice lacking PPARα depends on PPARα activity only in hepatocytes or also in other organs.

Here we investigated consequences of hepatocyte-specific *Pparα* deletion, focusing on effects on fatty acid metabolism in NAFLD, ranging from steatosis to steatohepatitis. We report the first evidence that adipocyte lipolysis correlates with and stimulates NAFLD when hepatocytes are lacking PPARα. Our data establish that hepatocyte-restricted *Pparα* deletion is sufficient to promote steatosis, emphasising this receptor's relevance as a drug target in NAFLD.

MATERIALS AND METHODS

Animals

Generation of *floxed-Pparα* mice and of *Pparα* hepatocyte-specific knockout ($Ppar\alpha^{hep-/-}$) animals is described in online supplementary file 1.

In vivo experiments

In vivo studies followed the European Union guidelines for laboratory animal use and care, and were approved by an independent ethics committee.

Detailed experimental protocols are provided in online supplementary file 1.

Plasma analysis

Plasma FGF21 and insulin, respectively, were assayed using the rat/mouse FGF21 ELISA kit (EMD Millipore) and the ultrasensitive mouse insulin ELISA kit (Crystal Chem) following the manufacturer's instructions. Aspartate transaminase, alanine transaminase (ALT), total cholesterol, LDL cholesterol and HDL cholesterol were determined using a COBAS-MIRA+ biochemical analyser (Anexplo facility).

Circulating glucose and ketone bodies

Blood glucose was measured using an Accu-Chek Go glucometer (Roche Diagnostics). β-Hydroxybutyrate content was measured using Optium β-ketone test strips with Optium Xceed sensors (Abbott Diabetes Care).

Histology

Paraformaldehyde-fixed, paraffin-embedded liver tissue was sliced into 5 µm sections and H&E stained. Visualisation was performed using a Leica DFC300 camera.

Liver lipids analysis

Detailed experimental protocols are provided in online supplementary file 1.

Gene expression studies

Total RNA was extracted with TRIzol reagent (Invitrogen). Transcriptomic profiles were obtained using Agilent Whole Mouse Genome microarrays (4×44k). Microarray data and experimental details are available in the Gene Expression Omnibus (GEO) database (accession number GSE73298 and GSE73299). For real-time quantitative PCR (qPCR), 2 µg RNA samples were reverse-transcribed using the High-Capacity cDNA Reverse Transcription Kit (Applied Biosystems). Online supplementary file 2 presents the SYBR Green assay primers. Amplifications were performed using an ABI Prism 7300 Real-Time PCR System (Applied Biosystems). qPCR data were normalised to TATA-box-binding protein mRNA levels, and analysed with LinRegPCR.v2015.3.

Transcriptomic data analysis

Data were analysed using R (http://www.r-project.org). Microarray data were processed using Bioconductor packages (http://www.bioconductor.org, v 2.12)[29] as described in GEO entry GSE26728. Further details are provided in online supplementary file 1.

Statistical analysis

Data were analysed using R (http://www.r-project.org). Microarray data were processed using bioconductor packages (http://www.bioconductor.org) as described in GEO entry GSE38083. Genes with a q value of <0.001 were considered differentially expressed between genotypes. Gene Ontology (GO) Biological Process enrichment was evaluated using conditional hypergeometric tests (GOstats package). For non-microarray data, differential effects were analysed by analysis of variance followed by Student's t-tests with a pooled variance estimate. A p value <0.05 was considered significant.

RESULTS

Generation of hepatocyte-specific PPARα knockout mice

Progeny carrying the $Ppar\alpha^{flox/flox}$ alleles (figure 1A), referred to as floxed, were backcrossed in the C57Bl/6J background, and then crossed with *albumin-Cre* mice in the same genetic background, generating a hepatocyte-specific PPARα knockout ($Ppar\alpha^{flox/flox}albumin\text{-}Cre^{+/-}$) referred to as $Ppar\alpha^{hep-/-}$ (figure 1B). PPARα mRNA was not detected in livers from $Ppar\alpha^{hep-/-}$ mice when compared with floxed and C57Bl6/J mice (figure 1C), suggesting that most hepatic PPARα expression is from hepatocytes. PPARα absence in hepatocytes did not alter mRNA expression of other PPAR isotypes (figure 1C).

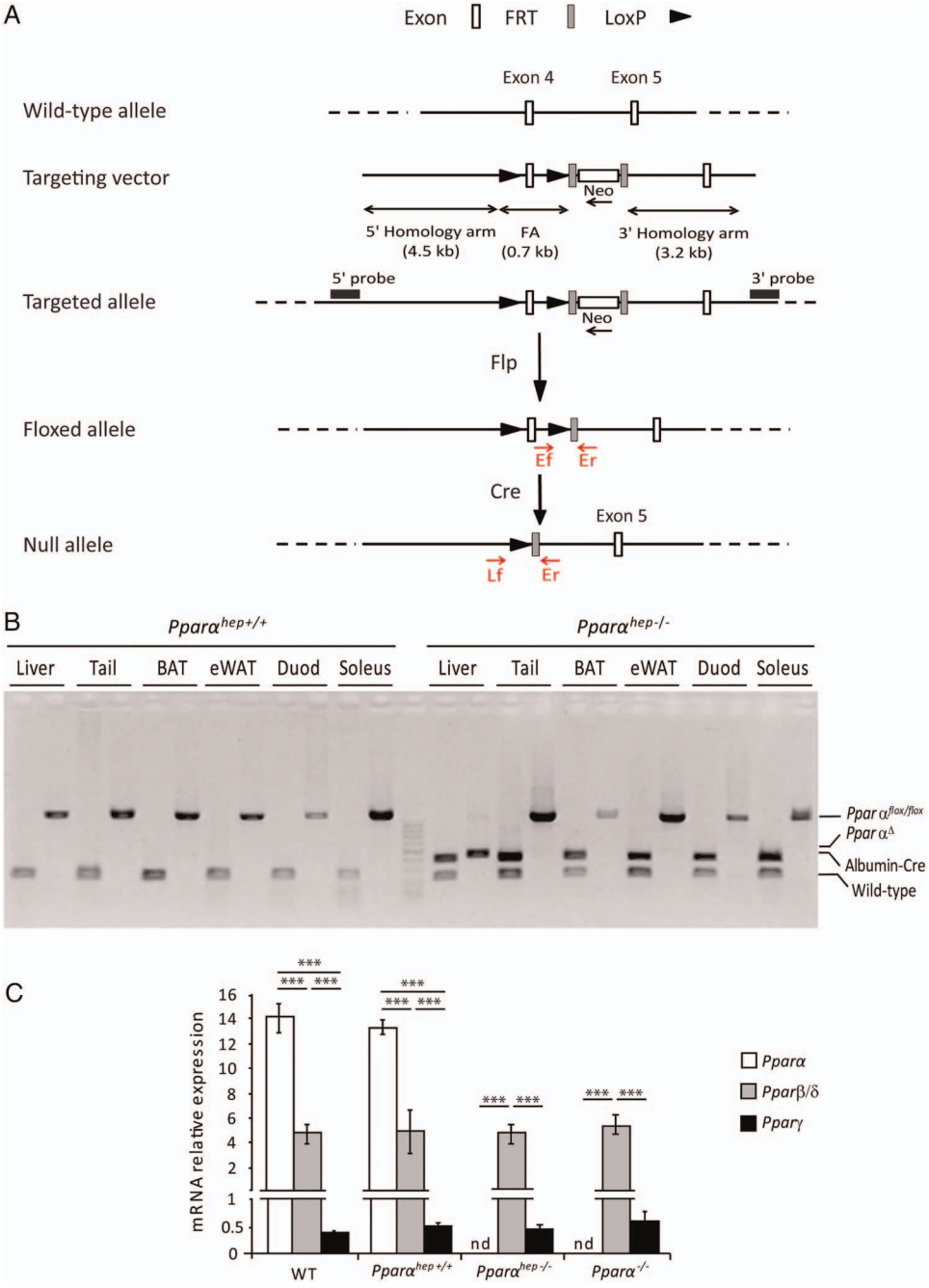

Figure 1 Characterisation of the hepatocyte-specific peroxisome proliferator-activated receptor α (PPARα) knockout mouse model. (A) Schematic of the targeting strategy to disrupt hepatic *Pparα* expression. (B) PCR analysis of *Pparα floxed* ($Ppar\alpha^{hep+/+}$) and *Albumin-Cre* ($Albumin\text{-}Cre^{+/-}$) genes from mice that are liver wild-type (WT), ($Ppar\alpha^{hep+/+}$) or liver knockout ($Ppar\alpha^{hep-/-}$) for *Pparα* using DNA extracted from different organs. (C) Relative mRNA expression levels of *Pparα*, *Pparβ/δ* and *Pparγ* from liver samples of WT, liver WT ($Ppar\alpha^{hep+/+}$), *Pparα* liver knockout ($Ppar\alpha^{hep-/-}$) and *Pparα* knockout ($Ppar\alpha^{-/-}$) mice (n=8 mice per group). Data represent mean±SEM. ***p≤0.005. FA, floxed allele; Flp, flippase; FRT, flippase recognition target; LoxP, locus of X-overP1; nd, not detected; PparαΔ, *Pparα* deletion; WT, the $Albumin\text{-}Cre^{-/-}$ allele.

Hepatocyte-autonomous effect of fenofibrate on PPARα activity

To determine whether PPARα response was hepatocyte-autonomous, we challenged wild-type (WT), floxed $Ppar\alpha^{hep+/+}$, $Ppar\alpha^{-/-}$ and $Ppar\alpha^{hep-/-}$ mice with the PPARα agonist fenofibrate. We measured mRNA expressions of PPARα target genes, including *Cyp4a10* (figure 2A) and *Cyp4a14* (figure 2B). Their expressions were strongly induced by fenofibrate in WT and in floxed $Ppar\alpha^{hep+/+}$ mice compared with $Ppar\alpha^{-/-}$ and $Ppar\alpha^{hep-/-}$ mice. These samples were also used for pangenomic expression profiling through microarray analysis (figure 2C). Differentially expressed gene (DEG) analysis was subjected to hierarchical clustering, highlighting similar expression profiles between WT and floxed $Ppar\alpha^{hep+/+}$ mice within fenofibrate-treated or vehicle-treated groups. Whole-body $Ppar\alpha^{-/-}$ and $Ppar\alpha^{hep-/-}$ mice were unresponsive to fenofibrate, suggesting that fenofibrate-induced hepatic changes were mainly due to autonomous hepatocyte responses, not secondary to extrahepatic PPARα activation. GO biological function analysis revealed that fenofibrate upregulated lipid metabolism, and repressed immune and defence response, metabolic responses, and glycosylation and glycoprotein metabolism (figure 2C, groups 1, 2, 6 and 7). However, untreated $Ppar\alpha^{-/-}$ and $Ppar\alpha^{hep-/-}$ mice showed marked differences (figure 2C, groups 3, 4, 8 and 9). This implies that the absence of extrahepatic PPARα has a significant impact on the liver transcriptional profile and underscores the relevance of $Ppar\alpha^{hep-/-}$ mice to define the hepatocyte autonomous role of the receptor in the control of liver function.

Hepatocyte PPARα activity is context-specific

The $Ppar\alpha^{hep-/-}$ model was used to determine whether PPARα could drive hepatic regulations both in fasting-induced fatty acid catabolism as well as fatty acid anabolism during refeeding. The

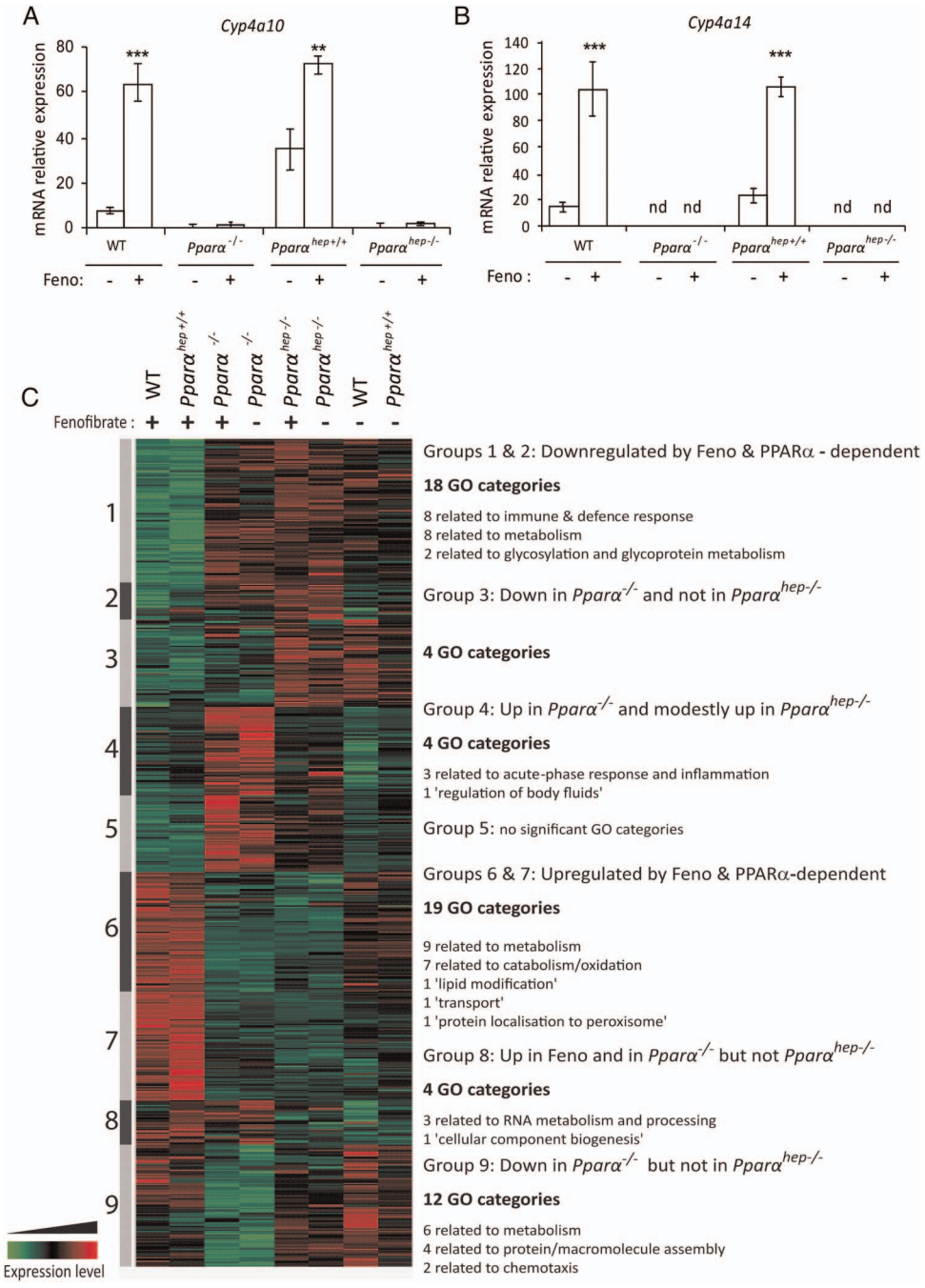

Figure 2 Pharmacological peroxisome proliferator-activated receptor α (PPARα) activation using fenofibrate reveals hepatocyte-specific PPARα-dependent biological functions. Liver samples from wild-type (WT), PPARα knockout (*Pparα*$^{-/-}$), liver WT (*Pparα*$^{hep+/+}$) and Pparα hepatocyte knockout (*Pparα*$^{hep-/-}$) mice treated with fenofibrate (Feno, +) or vehicle (–) by oral gavage for 14 days were collected. (A and B) The relative gene expression of two specific PPARα target genes *Cyp4a10* (A) and *Cyp4a14* (B) was measured by qRT-PCR. Data represent mean±SEM. **p≤0.01, ***p≤0.005. (C) Heat map representing data from a microarray experiment performed with liver samples. Hierarchical clustering is also shown, which allows the definition of nine gene clusters. Gene Ontology (GO) analysis of each cluster revealed significant biological functions (p≤0.05). nd, not detected.

fasting–refeeding experimental design was validated by measuring glycaemia (figure 3A) and expression of fatty acid synthase (*Fasn*), which encodes the rate-limiting enzyme in lipogenesis (figure 3B). Both were low during fasting, intermediary in ad libitum-fed animals, and high in refed animals. *Cyp4a14* (a well-known PPARα target) expression was low or undetectable in *Pparα*$^{hep-/-}$ animals, and strongly upregulated with fasting in WT mice (figure 3C).

Next we evaluated the hepatic transcriptome expression pattern using microarrays. We performed hierarchical clustering (figure 3D). Most PPARα-dependent changes were observed in fasted mouse livers. Venn diagrams were used to show nutritional status-related PPARα-dependent changes (figure 3E). Among the significant DEGs, 3048 were related to fasting, 390 to ad libitum-fed animals and 156 to refed mice, suggesting context-specific PPARα activity. The results further highlighted

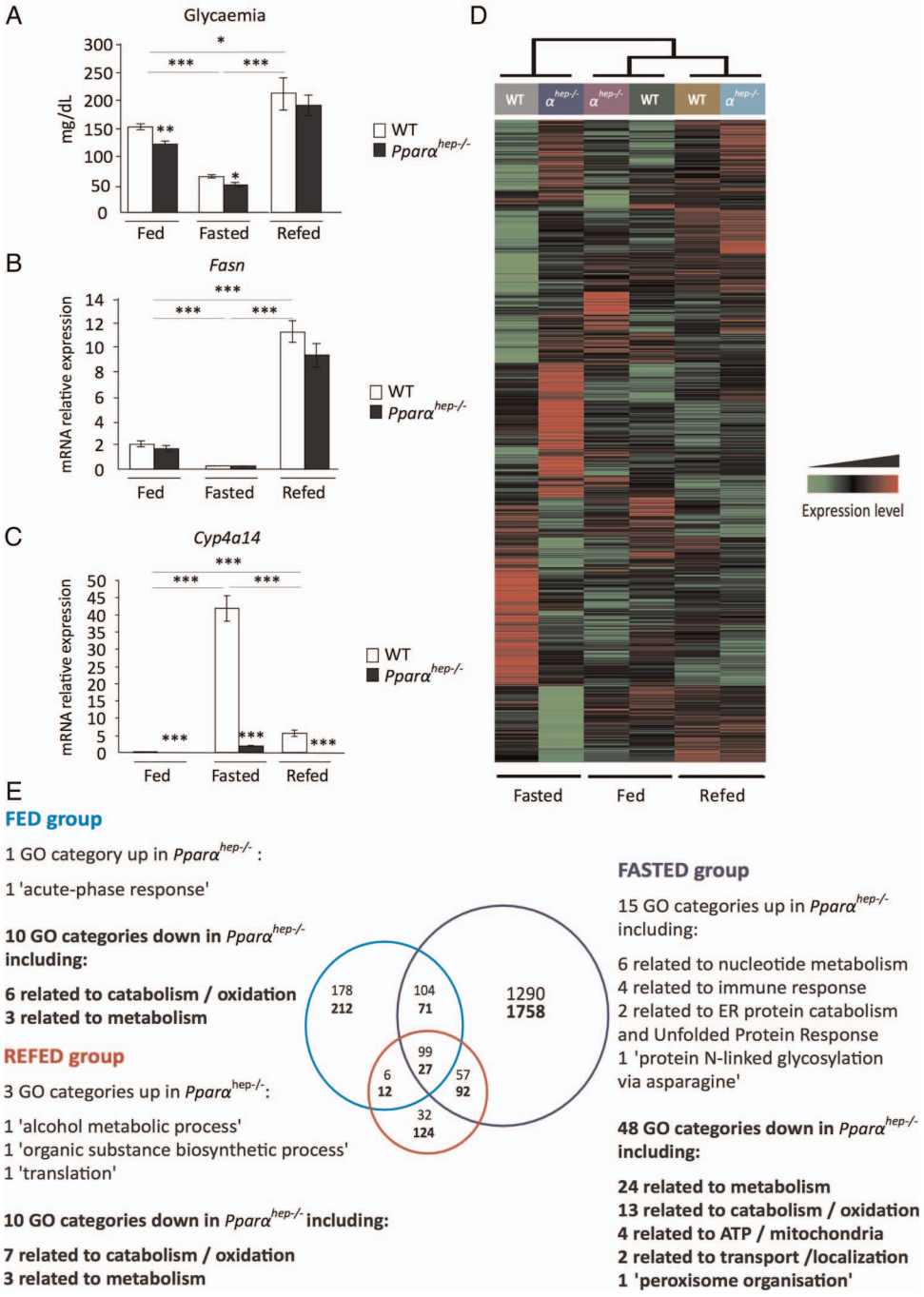

Figure 3 Hepatocyte-specific peroxisome proliferator-activated receptor α (PPARα) function is dependent on nutritional status. Wild-type (WT) and PPARα liver knockout (*Pparα*$^{hep-/-}$) male 8-week-old mice were fed ad libitum, fasted for 24 h, or fasted for 24 h and refed for 24 h. All mice were killed at ZT14, and sera and livers were collected. (A) Quantification of circulating glucose levels. (B, C) Relative mRNA expressions of *Fasn* (B) and *Cyp4a14* (C) in liver samples quantified by qRT-PCR. Data represent mean±SEM. *p≤0.05, **p≤0.01, ***p≤0.005. (D) Heat map was performed based on average gene expression levels from WT (n=12 (6 WT and 6 *Pparα*$^{hep+/+}$)) and from *Pparα*$^{hep-/-}$ (n=6). (E) Venn diagram and associated Gene Ontology (GO) function analysis (p≤0.05), GO categories corresponding to functions down in the absence of PPARα are in bold, GO categories corresponding to functions up in the absence of PPARα are in regular font.

that fasting, rather than feeding or refeeding, triggered the broader PPARα-dependent hepatocytic response, with most upregulated genes related to metabolism (figure 3E). However, the expression of several genes was identified as PPARα dependent regardless of the nutritional condition tested (fasting, but also feeding and refeeding). These genes are mostly downregulated in the absence of PPARα and pathway analysis highlights their involvement in mitochondrial fatty acid catabolism (see online supplementary file 3).

Biological function analyses revealed that both transcriptional activation and repression were PPARα sensitive (figure 3E). The functions of PPARα-sensitive repressions (GO categories up in *Pparα*$^{hep-/-}$ mice) varied with context, and included GO categories not directly related to metabolism, including acute-phase

response (fed), translation (refed) and protein glycosylation (fasted).

Hepatocyte PPARα is required for liver and whole-body fatty acid homeostasis in fasting

We next used $Ppar\alpha^{hep-/-}$ mice to determine the contribution of hepatocyte PPARα, and compared it with $Ppar\alpha^{-/-}$ and WT mice. We measured FFA and β-hydroxybutyrate (ketonaemia) levels in fasted and non-fasted mice (figure 4A). Plasma FFA was elevated in fasting mice of all three genotypes, but was significantly higher in $Ppar\alpha^{hep-/-}$ and $Ppar\alpha^{-/-}$ mice compared with controls. Fasting strongly increased ketone body levels in WT mice and to a lesser degree in $Ppar\alpha^{hep-/-}$ and $Ppar\alpha^{-/-}$ mice. This suggests that hepatic PPARα is required for FFA disposal and for β-hydroxybutyrate production. Correspondingly, fasting $Ppar\alpha^{hep-/-}$ and $Ppar\alpha^{-/-}$ mice showed elevated hepatic triglycerides and cholesterol esters (figure 4B), and substantial centrilobular steatosis (figure 4C), confirming that hepatic PPARα expression is required for fasting-induced FFA catabolism. PPARα absence led to defective expressions of PPARα target genes (figure 4D), including those involved in fatty acid catabolism and processing in lipid droplets (figure 4E). As a consequence of PPARα deficiency in hepatocytes, $Ppar\alpha^{hep-/-}$ mice exhibit a distinct fasting-induced fatty acid profile with a significant increase in oleic acid (C18:1n–9) and linoleic acid (C18:2n–6) when compared with WT mice (see online supplementary file 4).

Hepatocyte-specific *Pparα* deletion impairs constitutive and fasting-induced FGF21 expression

FGF21 is a hepatokine mainly produced by the liver. We examined liver *Fgf21* mRNA expression (figure 5A) and plasma FGF21 levels (figure 5B) in fed and fasted animals. We identified a constitutive expression peak during the day (ZT8) in both groups, and a fasting-triggered night-time peak (ZT16). In $Ppar\alpha^{hep-/-}$ mice, we examined whether fasting-induced FGF21 expression/production was strictly dependent on PPARα hepatic activity. $Ppar\alpha^{-/-}$ and $Ppar\alpha^{hep-/-}$ mice showed very low plasma FGF21 protein at ZT8 or at ZT16 with fasting (figure 5C).

Since FGF21 has been shown to reduce steatosis and lipotoxic lipids[13 30] we questioned whether the absence of FGF21 determines fasting-induced steatosis observed in $Ppar\alpha^{hep-/-}$ and $Ppar\alpha^{-/-}$ mice. FGF21 expression was rescued by adenoviral delivery both in $Ppar\alpha^{hep-/-}$ and in $Ppar\alpha^{-/-}$ mice (figure 5D). Comparable expression of FGF21 (figure 5E) was obtained in liver of WT, $Ppar\alpha^{hep-/-}$ and in $Ppar\alpha^{-/-}$ mice. FGF21-sensitive genes such as *G6pd* and *Scd1* showed significantly different expression in response to FGF21 overexpression (figure 5E). However, FGF21 only reduced hepatic triglycerides and cholesterol esters in WT mice, but not in $Ppar\alpha^{hep-/-}$ and in $Ppar\alpha^{-/-}$ mice (figure 5F, G). These results indicate that the fasting-induced steatosis occurring in $Ppar\alpha^{hep-/-}$ and in $Ppar\alpha^{-/-}$ mice does not depend on the lack of FGF21. This is in line with our observations that FGF21- and PPARα-sensitive target genes are different (see online supplementary file 5A). Moreover, it is also consistent with the observation that FGF21 overexpression does not rescue the expression of PPARα target genes and conversely that PPARα-sensitive regulations occur in $Fgf21^{-/-}$ mice (see online supplementary file 5B, C).

In addition to their defective fatty acid catabolism, $Ppar\alpha^{-/-}$ mice are hypoglycaemic and hypothermic during fasting.[7] Because FGF21 is important for glucose homeostasis and for thermogenesis,[13] we investigated the role of hepatocyte PPARα in controlling fasting glycaemia and body temperature. Both $Ppar\alpha^{hep-/-}$ and $Ppar\alpha^{-/-}$ mice were hypoglycaemic and hypothermic compared with WT mice during fasting. However, this phenotype was much stronger in fasted $Ppar\alpha^{-/-}$ mice compared with fasted $Ppar\alpha^{hep-/-}$ mice (figure 5H-J), indicating that extrahepatic PPARα strongly influenced whole-body glucose homeostasis and temperature independent of hepatocytic PPARα activity and FGF21 production.

Fasting-enhanced hepatocytic PPARα activity is time-restricted and sensitive to adipocyte lipolysis

We next tested the kinetics of other fasting-induced hepatic PPARα activity in vivo. We used several measures of PPARα activity, including *Fgf21* (figure 5A) and *Vanin1*, *Cyp4a10, Cyp4a14* and *Fsp27* mRNAs (figure 6A), since these genes were most sensitive to fasting and to fenofibrate, and were strictly PPARα dependent (see online supplementary files 6–10A). Plasma FFA and glucose levels were also measured during fasting (figure 6B). FFA were markedly increased in the early night (ZT14–ZT16). The FFA pattern was correlated with the PPARα mRNA expression profile and expressions of *Fgf21*, *Vanin1*, *Cyp4a10, Cyp4a14* and *Fsp27* (figures 5A and 6A). This strongly suggested that FFA released from adipocytes during fasting-influenced hepatic PPARα expression and activity without inflammatory response since hepatic *Tnfα* mRNA expression was not sensitive to fasting. We further determined that acute treatment of fasted mice with the β3-adrenergic receptor agonist CL316243 enhanced circulating FFA levels in WT and $Ppar\alpha^{hep-/-}$ mice (figure 6C), and increased expressions of *Fgf21*, *Cyp4a14*, *Vanin1*, *Cyp4a10* and *Fsp27* in WT mice but not $Ppar\alpha^{hep-/-}$ mice (figure 6D) without inducing Tnf α in response to fasting or in response to CL316243 (see online supplementary file 10C and D). These data support a role for acute adipocyte lipolysis as a signal for hepatocyte PPARα activity during fasting.

Hepatocyte PPARα is required for protection in steatohepatitis

We next examined whether the hepatocytic PPARα response to chronic lipolysis occurred during methionine-deficient and choline-deficient diet (MCD)-induced weight loss. In rodents, this diet rapidly promotes lipolysis in adipocytes, resulting in steatohepatitis. On the MCD diet, mice of each genotype showed weight loss (figure 7A), steatosis (figure 7B), and increased hepatic triglycerides, cholesterol esters (figure 7C) and plasma ALT (figure 7D). Compared with WT, $Ppar\alpha^{hep-/-}$ and $Ppar\alpha^{-/-}$ mice showed greater steatosis and liver damage, suggesting a more severe MCD diet-induced phenotype without hepatocyte PPARα. MCD also induced increased expressions of *Cyp4a14* and *Vanin1* in WT mice, but not $Ppar\alpha^{hep-/-}$ or $Ppar\alpha^{-/-}$ mice (figure 7E). *Fgf21* mRNA (figure 7E) and circulating FGF21 (figure 7F) were increased through a mechanism that is partly dependent on hepatic PPARα. Overall, hepatocyte-specific *Pparα* deletion aggravated MCD diet-induced liver damage, correlating with defective PPARα-dependent pathway upregulation in response to chronic lipolysis.

Additionally, we questioned whether hepatocyte PPARα may also be required for the protection of the liver during early hits in steatosis such as those occurring in response to short-term exposure to a high-fat diet (HFD). Over 2 weeks of HFD, mouse liver accumulated hepatic triglycerides and cholesterol esters. Importantly, this steatosis was twice higher in $Ppar\alpha^{hep-/-}$ mice than in WT mice, and was further elevated in $Ppar\alpha^{-/-}$ mice (see online supplementary file 11). Altogether, these data suggest that hepatic PPARα is essential in hepatoprotection.

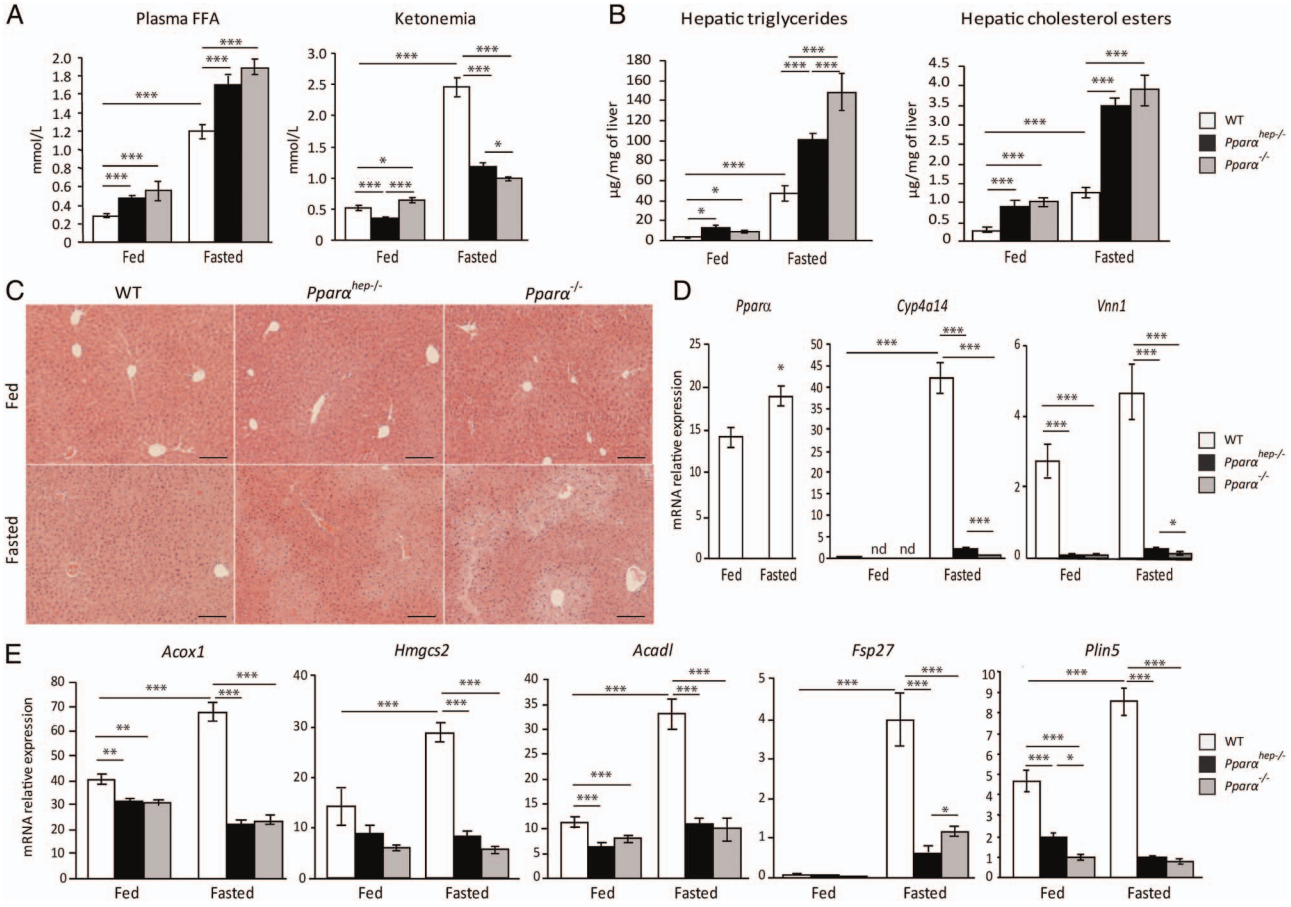

Figure 4 Fasting is the major inducer of hepatic peroxisome proliferator-activated receptor α (PPARα) activity. Wild-type (WT), hepatocyte-specific PPARα knockout (*Pparα*$^{hep-/-}$) and total PPARα knockout (*Pparα*$^{-/-}$) mice were fed ad libitum or fasted for 24 h and then killed. (A) Quantification of plasma free fatty acids (FFAs) and ketone bodies (ketonaemia). (B) Hepatic triglycerides and cholesterol esters hepatic levels. (C) Representative pictures of H&E staining of liver sections. Scale bars, 100 µm. (D) Relative mRNA expression levels of *Pparα*, *Cyp4a14* and *Vnn1* in liver samples determined by qRT-PCR. (E) Quantification of mRNA expression of *Acox1*, *Hmgcs2*, *Acadl*, *Fsp27* and *Plin5* by qRT-PCR. Data shown as mean±SEM. *p≤0.05, **p≤0.01, ***p≤0.005.

Hepatocyte PPARα deficiency leads to steatosis and hypercholesterolaemia but not excess weight gain in ageing mice

Lastly, we questioned the long-term consequences of hepatocyte-specific *Pparα* deletion during ageing. More specifically, since PPARα is broadly expressed in metabolic tissues, we aimed at clarifying whether the steatosis that develops in aged whole-body *Pparα*$^{-/-}$ mice is due to the hepatocytic defect in PPARα activity. WT, *Pparα*$^{hep-/-}$ and *Pparα*$^{-/-}$ mice were fed a standard diet over 1 year. *Pparα*$^{-/-}$ mice, but not *Pparα*$^{hep-/-}$ mice, grew overweight with ageing (figure 8A–C). Both *Pparα*$^{hep-/-}$ and *Pparα*$^{-/-}$ mice showed spontaneous centrilobular steatosis (figure 8D), elevated hepatic triglycerides and hepatic cholesterol esters (figure 8E), as well as hypercholesterolaemia (see figure 8F online supplementary file 12) without hyperglycaemia (figure 8G). Overall, hepatocyte-specific PPARα deficiency was sufficient to induce spontaneous steatosis and disrupt whole-body fatty acid as well as cholesterol homeostasis, but did not affect weight gain and diabetes during ageing.

DISCUSSION

NAFLD are a spectrum of diseases presenting a major public health concern that is strongly linked with obesity. Most accumulated hepatic fatty acids in NAFLD come from increased non-esterified FFA in the fasting state.[17] Thus, it is essential to define the mechanisms by which the liver adapts to this influx. FFA processing largely involves the fatty acid oxidative pathway, coupled to ketogenesis allowing the liver to use lipids,[31] which is critical during fasting and requires transcriptional regulation of rate-limiting enzymes.[32]

Whole-body *Pparα*$^{-/-}$ mice show impaired coping with prolonged fasting, resulting in defective fatty acid oxidation and steatosis, hypoglycaemia and hypothermia. However, PPARα also contributes to metabolic homeostasis through expression in other tissues. Here we investigated the impact of hepatocyte-specific PPARα deletion on liver physiology and lipid metabolism in vivo. To our knowledge, this is the first report that selective PPARα deletion in hepatocytes (*Pparα*$^{hep-/-}$) was sufficient to promote hepatic steatosis.

PPARα is targeted by several fibrate drugs,[33] and by pan-agonists for PPAR isotypes[21] that are currently in clinical trials for NASH treatment. Using *Pparα*$^{hep-/-}$ mice, we demonstrated an autonomous transcriptional response of hepatocytes to fenofibrate, indicating that fibrates' effects on the liver gene expression are largely independent from those in extrahepatic tissues. Moreover, liver gene expression profiles markedly differed between untreated *Pparα*$^{-/-}$ and *Pparα*$^{hep-/-}$ mice, suggesting that extrahepatocytic PPARα activity substantially influenced the hepatic transcriptome.

Food restriction induces PPARα activity, and endogenous PPARα ligand production requires hepatic lipogenesis, which

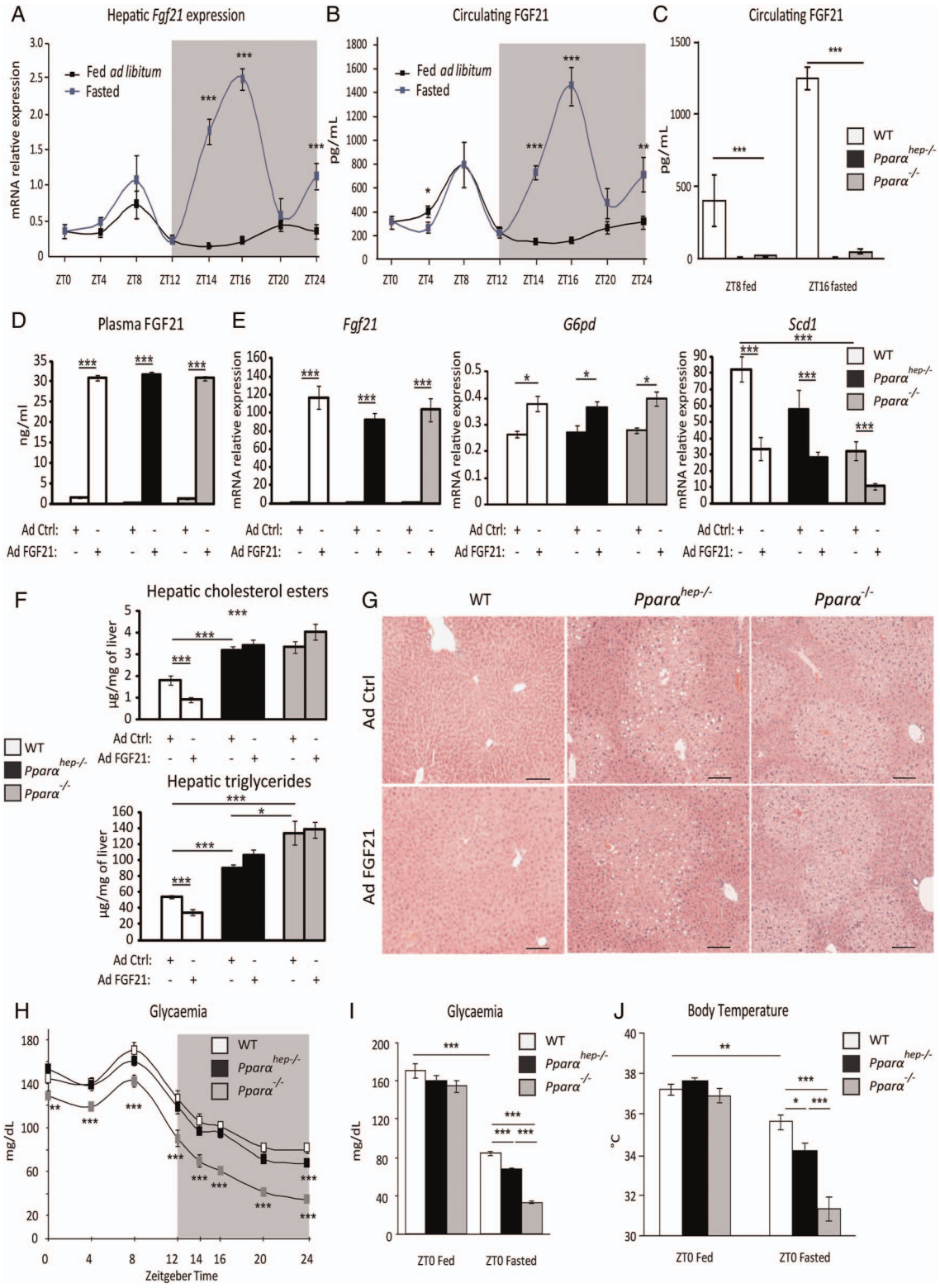

Figure 5 Hepatocyte and extrahepatocyte peroxisome proliferator-activated receptor α (PPARα) regulate fibroblast growth factor 21 (FGF21), glycaemia and body temperature during fasting. (A and B) Eleven-week-old male mice of the C57Bl/6J background were fed ad libitum or fasted for 24 h, and were killed around the clock from ZT0 to ZT24. (A) *Fgf21* mRNA was quantified by qRT-PCR. (B) Quantification of circulating FGF21 levels by ELISA. (C) Twelve-week-old wild-type (WT), PPARα-hepatocyte knockout ($Ppar\alpha^{hep-/-}$) and PPARα knockout ($Ppar\alpha^{-/-}$) male mice were fed ad libitum or fasted for 16 h and blood was collected at ZT8 (ZT8 fed) or at ZT16 (ZT16 fasted). FGF21 plasma level was determined by ELISA. (D–G) Male mice of WT, $Ppar\alpha^{hep-/-}$ and $Ppar\alpha^{-/-}$ genotypes were infected with an adenoviral construct containing cDNA of Fgf21 or an empty vector. Mice were sacrificed after a 24 h fasting period at ZT14. (D) Quantification of circulating FGF21 levels by ELISA. (E) *Fgf21*, *G6pd* and *Scd1* mRNAs were quantified by qRT-PCR. (F) Quantification of hepatic cholesterol esters and triglycerides. (G) Representative pictures of H&E staining of liver sections. Scale bars, 100 µm. (H) Plasma glucose level was monitored over a 24 h fasting period from ZT0 to ZT24 in WT, $Ppar\alpha^{hep-/-}$ and $Ppar\alpha^{-/-}$ mice. (I, J) Plasma glucose (I) and body temperature (J) were determined at ZT0 in fed mice or at ZT0 in mice fasted for 24 h. Data are shown as mean±SEM. *p≤0.05, **p≤0.01, ***p≤0.005.

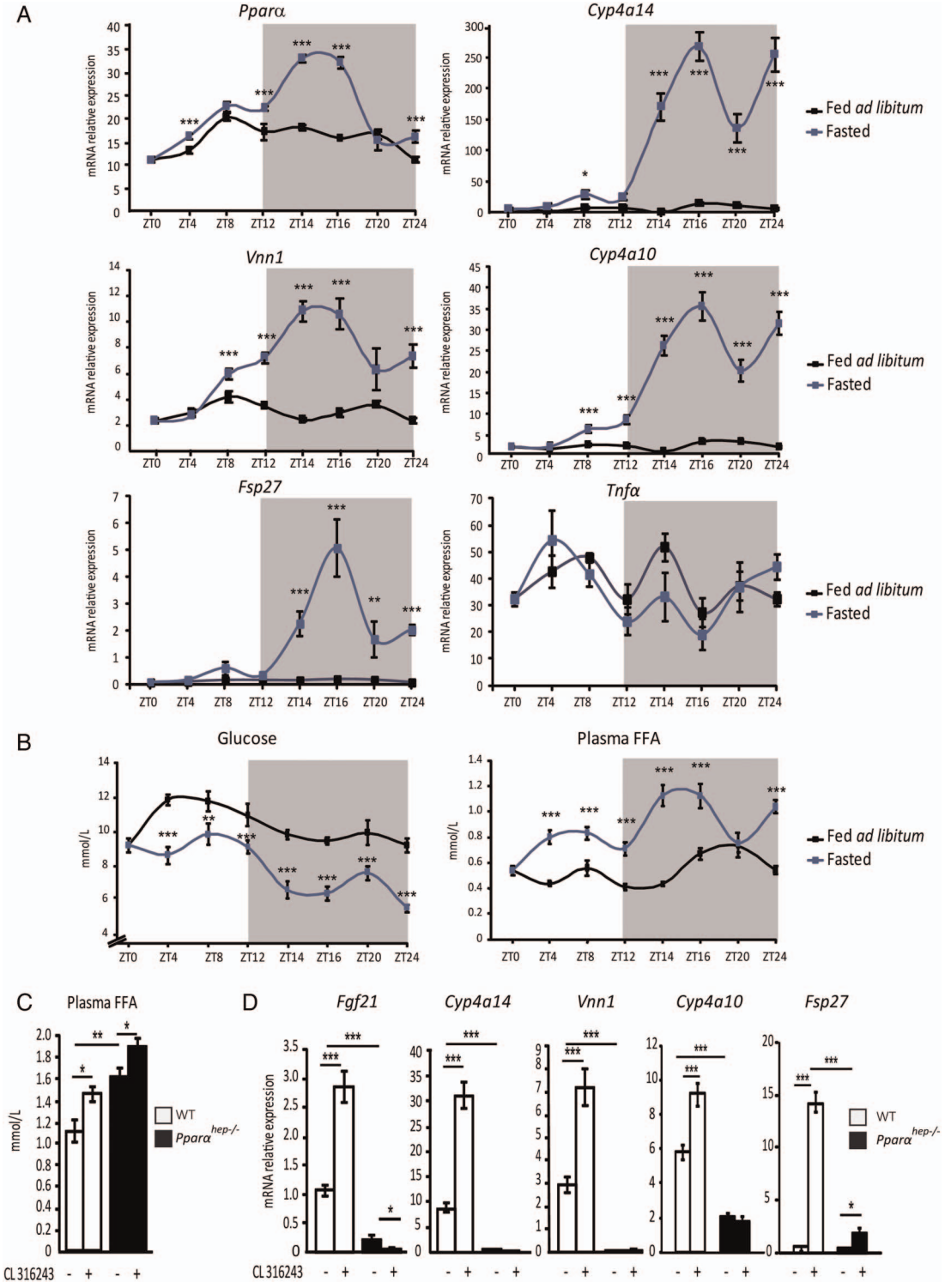

Figure 6 Hepatocyte peroxisome proliferator-activated receptor α (PPARα) activity is induced by adipose tissue lipolysis. (A and B) Liver samples were collected from male wild-type (WT) C57Bl/6J mice that were fed ad libitum (black curve) or fasted (blue curve) over 24 h. (A) Hepatic mRNA expression levels of *Pparα*, *Cyp4a14*, *Vnn1*, *Cyp4a10, Fsp27 and Tnfα* were quantified by qRT-PCR. (B) Plasma glucose and free fatty acids (FFA) were measured. (C and D) WT and PPARα hepatocyte-specific knockout ($Ppar\alpha^{hep-/-}$) mice were treated with the β3-adrenergic receptor agonist CL316243 at ZT6 and then killed at ZT14. (C) Quantification of plasma FFA. (D) Relative mRNA expression levels of *Fgf21*, *Cyp4a14*, *Vnn1*, *Cyp4a10* and *Fsp27* were measured by qRT-PCR. Data are shown as mean±SEM. *p≤0.05, **p≤0.01, ***p≤0.005.

increases upon feeding.[34 35] Thus, PPARα may be important during fasting-induced lipid catabolism and in the response to anabolic fatty acid-derived signals. Our data revealed the context dependency of PPARα hepatocytic activity defined by DEGs. This activity was clearly the highest during fasting. During fasting, hepatocyte-specific PPARα deletion resulted in steatosis, increased plasma FFA and impaired ketone bodies. This supports the concept that FFA released from adipose stores during fasting may activate PPARα for hepatic use. Accordingly, we found that $Ppar\alpha^{hep-/-}$ mice accumulate high oleic and

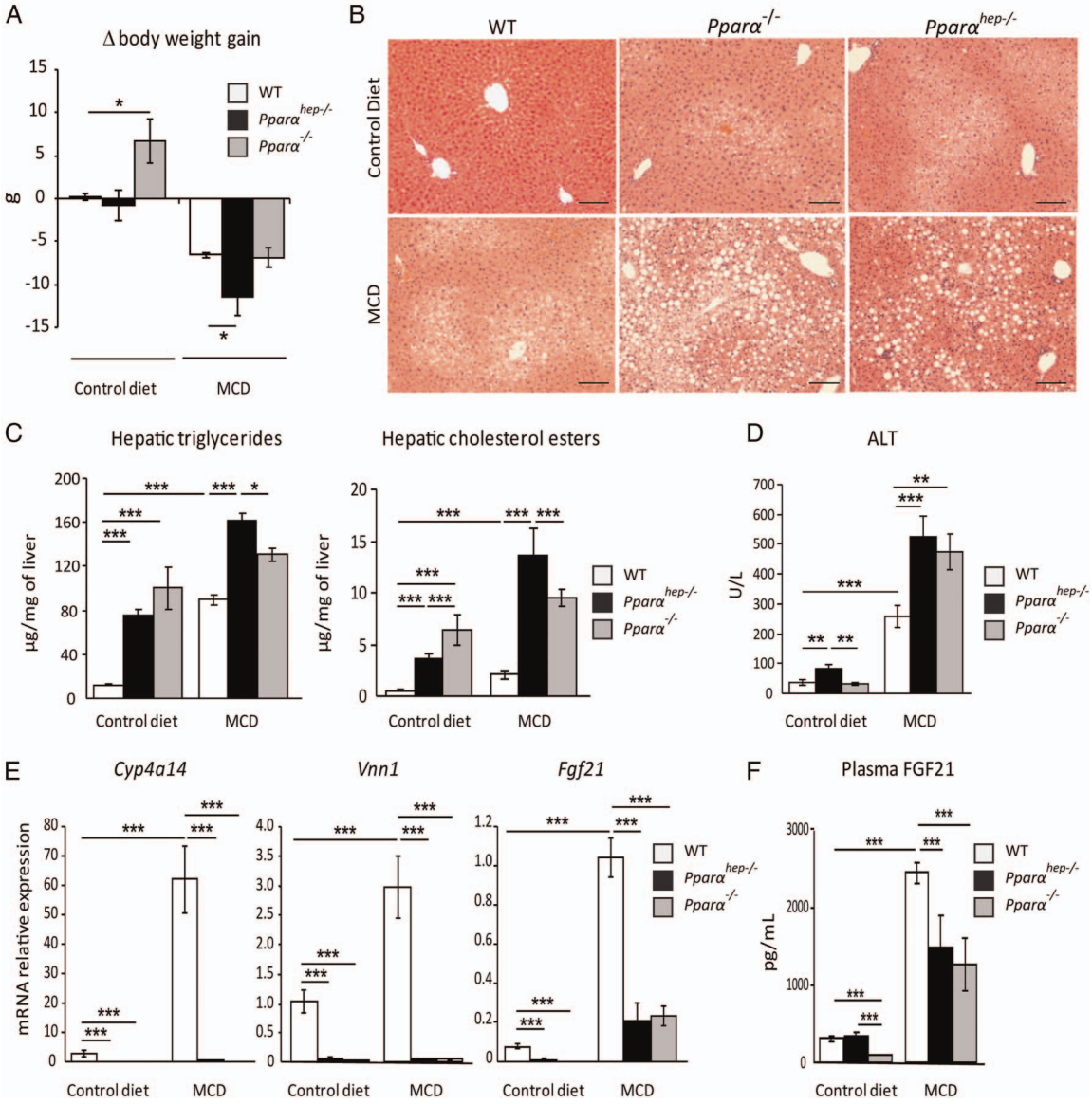

Figure 7 Liver peroxisome proliferator-activated receptor α (PPARα) deficiency aggravates non-alcoholic steatohepatitis in response to a methionine-deficient and choline-deficient diet (MCD). Wild-type (WT), PPARα hepatocyte knockout (*Pparα*$^{hep-/-}$) and PPARα knockout (*Pparα*−/−) mice were fed a MCD or a control diet for 2 weeks and were killed at ZT8. (A) Body weight gain was measured over 2 weeks. (B) Representative pictures of H&E staining on liver sections. Scale bar, 100 µm. (C) Quantification of hepatic triglycerides and cholesterol esters. (D) Alanine transaminase activity level in plasma. (E) Hepatic mRNA expression levels of *Cyp4a14*, *Vnn1* and *Fgf21*. (F) Plasma levels of fibroblast growth factor 21 (FGF21). Data are shown as mean±SEM. *p≤0.05, **p≤0.01, ***p≤0.005.

linolenic acids in the liver during fasting (see online supplementary file 4), which is in agreement with the fact that both of them are the main fatty acids stored in the white adipose tissues of mice fed a chow diet.[36] Importantly, we found a high correlation between the kinetics of circulating FFA increase and expression of PPARα and several of its target genes. Moreover, treatment with a β3-adrenergic receptor agonist further enhanced this response in vivo through PPARα but did not induce detrimental FFA-sensitive response driven by toll-like receptor 4 (TLR4). This is likely due to the mixture of FFA released from the adipose stores. Indeed, fatty acids that accumulated in the liver of *Pparα*$^{hep-/-}$ mice during fasting were mostly oleic (C18:1n–9) and linoleic acids (C18:2n–6), and not only saturated fatty acids such as palmitic acid (C16:0). Interestingly, it has been shown that palmitic acid cannot activate TLR4 in the presence of unsaturated FFA.[37]

Overall, our data highlight hepatic PPARα activity regulation by fatty acids released from adipocytes. This contrasts with the previous evidence that PPARβ/δ rather than PPARα may act as a FFA sensor.[38] However, our data support the possibility that this adipose-derived signal is time-restricted and specifically efficient in early night. Moreover, other pathways likely influence PPARα activity by providing ligands.[34 35 39 40] Several insulin-sensitive signalling mechanisms influence hepatic PPARα, and adipocyte lipolysis is insulin sensitive.[41] Thus, insulin may coordinate hepatic PPARα, both through cell-autonomous mechanisms and adipocyte lipolysis inducing interorgan communication mediated by FFA release. Our findings also correspond with the recent evidence that adipocyte lipolysis may regulate hepatic *Fgf21*.[42] Circulating FGF21 was strictly dependent on hepatocytic PPARα activation during fasting. Most circulating FGF21 is liver-derived[43] and *Pparα*$^{-/-}$ mice

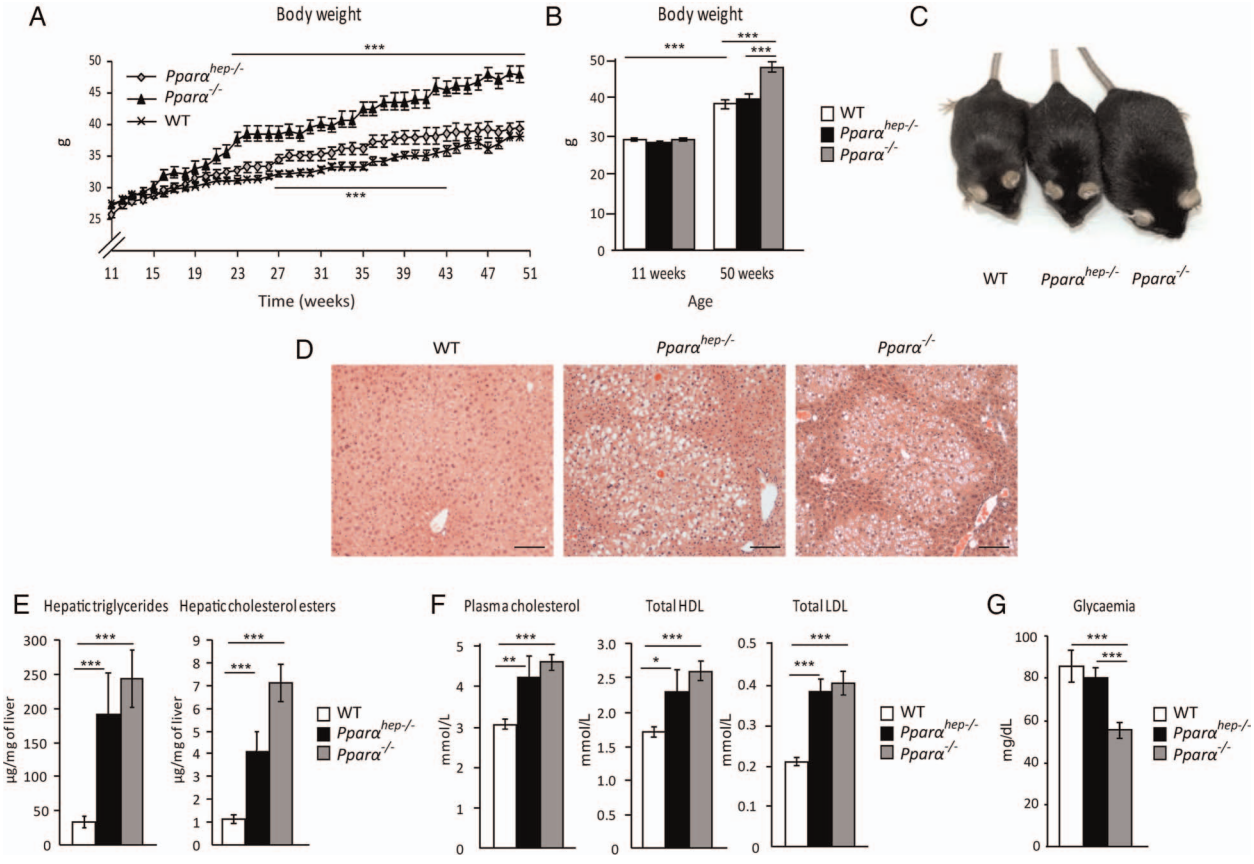

Figure 8 Mice deficient in hepatic peroxisome proliferator-activated receptor α (PPARα) develop spontaneous hepatic steatosis during ageing. Wild-type (WT), PPARα hepatocyte knockout (*Pparα*$^{hep-/-}$) and PPARα knockout (*Pparα*$^{-/-}$) mice were fed a chow diet for 51 weeks. All mice were killed at ZT16 in a non-fasted state. (A) Body weight gain was followed over time. (B) Comparison of body weight between weeks 11 and 50. (C) Representative pictures of 52-week-old mice of the three genotypes. (D) Representative images of H&E staining of liver sections. Scale bar, 100 µm. (E) Quantification of hepatic triglycerides and cholesterol esters. (F) Measurement of plasma total cholesterol, HDL cholesterol and LDL cholesterol. (G) Fasting glycaemia. Data are shown as mean±SEM. *p≤0.05, **p≤0.01, ***p≤0.005.

show very little FGF21.[11 12] Other transcription factors can also regulate hepatic *Fgf21* expression[44–48] and PPARα is also expressed in extrahepatic tissues.[13] Our findings in *Pparα*$^{hep-/-}$ mice showed very little FGF21 without hepatic PPARα in both fed and fasted states. *Pparα*$^{-/-}$ mice are hypoglycaemic and hypothermic during fasting[7] and FGF21 is known for its endocrine effect on glucose homeostasis and thermogenesis.[13] However, compared with fasted *Pparα*$^{-/-}$ mice, fasted *Pparα*$^{hep-/-}$ mice showed reduced hypoglycaemia and hypothermia while FGF21 was equally absent in both models. This indicates that extrahepatocytic PPARα strongly influenced whole-body glucose homeostasis and temperature independently of hepatocyte PPARα and FGF21 production during fasting. In addition, while FGF21 prevents steatosis in different mouse models[13 30] and FGF21 reduces hepatic lipids in WT mice, its overexpression is not sufficient to protect from lipid accumulation in *Pparα*$^{hep-/-}$ and in *Pparα*$^{-/-}$ mice. Therefore, the absence of FGF21 is not the primary cause for the steatosis observed in *Pparα*$^{hep-/-}$ mice.

Lack of hepatic PPARα impairs the liver's ability to use FFA from acute lipolysis, resulting in steatosis. MCD diet-induced weight loss[49 50] also correlated with hepatic PPARα activity, suggesting that chronic lipolysis elevates hepatocytic PPARα activity in non-fasted mice. In agreement with the findings in whole-body PPARα-deficient mice,[20] our data demonstrated that the absence of hepatocytic PPARα was sufficient to increase MCD diet-induced liver damage. FGF21 expression/circulating levels increased in steatohepatitis, supporting the possibility that elevated FGF21 may reflect liver stress without fasting. This MCD diet-induced FGF21 increase was not strictly PPARα-dependent, consistent with the findings that amino acid deprivation induces hepatic FGF21 expression through ATF4.[44] PPARα presence led to greater FGF21 increase, and may contribute to hepatoprotection from lipotoxic lipid accumulation.[30]

MCD diet is widely used for preclinical NASH studies. However, it has many limitations, including the important weight loss that occurs in mice fed such diet. Therefore, we also tested the role of hepatocyte PPARα in lipid homeostasis in response to a short-term HFD feeding, which is sufficient to initiate early neutral lipid accumulation that may promote NAFLD. *Pparα*$^{hep-/-}$ mice showed marked increase in hepatic steatosis in response to 2 weeks of HFD feeding (see online supplementary file 11) suggesting that hepatocyte PPARα plays a dual role in exogenous (dietary) as well as in endogenous (released from adipocyte lipolysis) fatty acid homeostasis.

Previous studies have shown that *Pparα*$^{-/-}$ mice show a significant alteration of systemic lipid metabolism that leads to hepatic steatosis in ageing mice. Since PPARα is active in skeletal muscles,[23] adipose tissues,[24 25] intestines,[26] kidneys[27] and heart,[28] which all contribute to fatty acid homeostasis, it is impossible to determine whether the spontaneous steatosis that occurs in ageing *Pparα*$^{-/-}$ mice originates from a defect in the hepatocytic PPARα activity. This led us to investigate ageing-related differences between *Pparα*$^{-/-}$ and *Pparα*$^{hep-/-}$

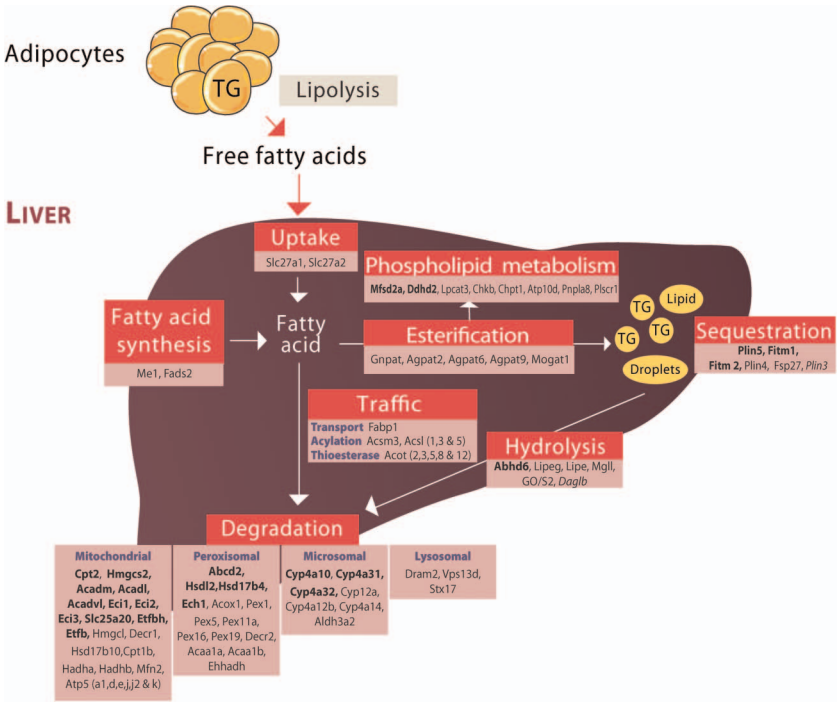

Figure 9 Overview of hepatocyte-specific peroxisome proliferator-activated receptor α (PPARα)-regulated genes involved in fatty acid metabolism. This figure was designed based on transcriptome analysis of PPARα-dependent gene expression in hepatocytes. Genes listed in regular font are induced by fenofibrate and by fasting in wild-type (WT) but not in *Pparα*$^{hep-/-}$ mice. Genes in italics are repressed by fenofibrate and by fasting in WT but not in *Pparα*$^{hep-/-}$ mice. Genes referenced in bold are downregulated in *Pparα*$^{hep-/-}$ compared with WT mice, whatever the conditions.

mice. During ageing, *Pparα*$^{-/-}$ mice became overweight and developed steatosis, while *Pparα*$^{hep-/-}$ mice only suffered steatosis. Therefore, neither obesity nor hyperglycaemia, which are both known to promote NAFLD,[15 16] is responsible for the steatosis observed in mice with hepatocyte-specific PPARα deletion.

Furthermore, both *Pparα*$^{-/-}$ and *Pparα*$^{hep-/-}$ ageing mice were hypercholesterolaemic. This is likely due to the dysregulation of apolipoproteins gene expression as well as cholesterol transport (Abcg8) as revealed in microarray analysis (see online supplementary file 12A). It is also possible that the cholesterol biosynthesis pathway driven by SREBP-2 may be dysregulated in the absence of PPARα since some of the SREBP-2 genes are elevated in *Pparα*$^{-/-}$ and/or in *Pparα*$^{hep-/-}$ mice (see online supplementary file 12B). Therefore, this suggests that drugs that activate hepatocytic PPARα will likely influence whole-body fatty acid and cholesterol homeostasis.

Altogether, our extensive analysis performed in *Pparα*$^{hep-/-}$ mice has allowed us to extend the evidence for the central role of PPARα in hepatocyte fatty acid homeostasis (figure 9). PPARα is strikingly essential to many aspects of fatty acid homeostasis including degradation through oxidative pathways. Our work provides the first demonstration that hepatocyte-specific PPARα deletion impairs whole-body fatty acid homeostasis during fasting, MCD and HFD feeding as well as in ageing. These findings underscore the central role of PPARα in the clearance of dietary fatty acids and of FFA released from adipocytes, the major source of lipid accumulation in NAFLD. These data highlight the relevance of PPARα as a drug target for NAFLD treatment.

Author affiliations
[1]INRA UMR1331, ToxAlim, University of Toulouse, Toulouse, France
[2]INSERM UMR 1048, Institute of Metabolic and Cardiovascular Diseases, Toulouse, France
[3]University of Toulouse, UMR1048, Paul Sabatier University, France
[4]INSERM U1016, Cochin Institute, Paris, France
[5]CNRS UMR 8104, Paris, France
[6]University of Paris Descartes, Sorbonne Paris Cité, Paris, France
[7]INSERM/UPS-US006/CREFRE, Service d'Histopathologie, CHU Purpan, Toulouse, France
[8]INSERM U855, University of Lyon, Lyon, France
[9]INRA UMR1348 Pegase, Saint-Gilles, France
[10]Agrocampus Ouest, UMR1348 Pegase, Rennes, France
[11]Université Européenne de Bretagne, France
[12]Laboratory of Clinical Biochemistry, Toulouse University Hospitals, Toulouse, France
[13]Lee Kong Chian School of Medicine, Nanyang Technological University, Singapore, Singapore
[14]Center for Integrative Genomics, University of Lausanne, Genopode Building, Lausanne, Switzerland

Acknowledgements We thank all members of the EZOP staff, particularly Colette Bétoulières for her careful and outstanding help from the early start of this project. We thank Aurore Dequesnes and Laurent Monbrun for their excellent work on plasma biochemistry. We thank Christine Salon and Florence Capilla for their excellent work on histology. We thank the staff from the Genotoul: Anexplo, Get-TriX and Metatoul-Lipidomic facilities. The authors wish to thank Professor Daniel Metzger, Professor Pierre Chambon (IGBMC, Illkirch, France) and the staff of the Mouse Clinical Institute (Illkirch, France) for their critical support in this project. We thank Professor Didier Trono (EPFL, Lausanne, Switzerland) for providing us with the Albumin-cre mice. We thank Professor David Mangelsdorf (Howard Hughes Medical Institute, Dallas, TX) and Professor Steven Kliewer (UT Southwestern, Dallas, TX) for providing us with the FGF21-deficient mice. We thank Alice Marmugi and Géraldine Michel for their technical assistance. We thank Professor Bertrand Cariou and Professor Bart Staels for constructive discussions.

Contributors AM initiated the project, designed experiments, performed experiments, analysed the data and wrote the paper. AP, EF, SD, YL, FL, MR, CL, FB and AI contributed to design experiments, perform experiments and to analyse the data. VB designed and performed a critical experiment. JB-M, TAS, PC and LL provided critical analysis and technical support. SL contributed to analyse the data. GM, FR and TP provided critical materials and contributed to design the project. NL, CP and DL critically contributed to design the project and supervised experiments. WW provided critical reagents, designed the project, analysed the data and wrote the paper. HG designed the project, performed experiments, analysed the data and wrote the paper.

Funding This work was funded by grants from the Human Frontier Science Program (HFSP) (WW), by Start-Up Grants from the Lee Kong Chian School of Medicine, Nanyang Technological University, Singapore (to WW), by SFN (to HG), by ANRs 'Crisalis' (to CP and HG), by 'Obelip' (to DL, CP, AM and HG). DL is a member of the Institut Universitaire de France. AM, DL, WW and HG were supported by Région Midi-Pyrénées.

Competing interests None declared.

Provenance and peer review Not commissioned; externally peer reviewed.

Data sharing statement Gene expression array raw data are deposited in GEO as indicated in the manuscript.

REFERENCES

1 Browning JD, Horton JD. Molecular mediators of hepatic steatosis and liver injury. *J Clin Invest* 2004;114:147–52.
2 Wahli W, Michalik L. PPARs at the crossroads of lipid signaling and inflammation. *Trends Endocrinol Metab* 2012;23:351–63.
3 Braissant O, Foufelle F, Scotto C, *et al*. Differential expression of peroxisome proliferator-activated receptors (PPARs): tissue distribution of PPAR-alpha, -beta, and -gamma in the adult rat. *Endocrinology* 1996;137:354–66.
4 Postic C, Girard J. Contribution of de novo fatty acid synthesis to hepatic steatosis and insulin resistance: lessons from genetically engineered mice. *J Clin Invest* 2008;118:829–38.
5 Kersten S. Integrated physiology and systems biology of PPARα. *Mol Metab* 2014;3:354–71.
6 Lee SS, Pineau T, Drago J, *et al*. Targeted disruption of the alpha isoform of the peroxisome proliferator-activated receptor gene in mice results in abolishment of the pleiotropic effects of peroxisome proliferators. *Mol Cell Biol* 1995;15:3012–22.
7 Kersten S, Seydoux J, Peters JM, *et al*. Peroxisome proliferator-activated receptor alpha mediates the adaptive response to fasting. *J Clin Invest* 1999;103:1489–98.
8 Kroetz DL, Yook P, Costet P, *et al*. Peroxisome proliferator-activated receptor α controls the hepatic CYP4A induction adaptive response to starvation and diabetes. *J Biol Chem* 1998;273:31581–9.
9 Patsouris D, Mandard S, Voshol PJ, *et al*. PPARalpha governs glycerol metabolism. *J Clin Invest* 2004;114:94–103.
10 Lee JM, Wagner M, Xiao R, *et al*. Nutrient-sensing nuclear receptors coordinate autophagy. *Nature* 2014;516:112–15.
11 Badman MK, Pissios P, Kennedy AR, *et al*. Hepatic fibroblast growth factor 21 is regulated by PPARalpha and is a key mediator of hepatic lipid metabolism in ketotic states. *Cell Metab* 2007;5:426–37.
12 Inagaki T, Dutchak P, Zhao G, *et al*. Endocrine regulation of the fasting response by PPARalpha-mediated induction of fibroblast growth factor 21. *Cell Metab* 2007;5:415–25.
13 Kharitonenkov A, Adams AC. Inventing new medicines: The FGF21 story. *Mol Metab* 2014;3:221–9.
14 Pawlak M, Lefebvre P, Staels B. Molecular mechanism of PPARα action and its impact on lipid metabolism, inflammation and fibrosis in non-alcoholic fatty liver disease. *J Hepatol* 2015;62:720–33.
15 Loomba R, Sanyal AJ. The global NAFLD epidemic. *Nat Rev Gastroenterol Hepatol* 2013;10:686–90.
16 Wree A, Broderick L, Canbay A, *et al*. From NAFLD to NASH to cirrhosis-new insights into disease mechanisms. *Nat Rev Gastroenterol Hepatol* 2013;10:627–36.
17 Donnelly KL, Smith CI, Schwarzenberg SJ, *et al*. Sources of fatty acids stored in liver and secreted via lipoproteins in patients with nonalcoholic fatty liver disease. *J Clin Invest* 2005;115:1343–51.
18 Abdelmegeed MA, Yoo SH, Henderson LE, *et al*. PPARalpha expression protects male mice from high fat-induced nonalcoholic fatty liver. *J Nutr* 2011;141:603–10.
19 Costet P, Legendre C, Moreé J, *et al*. Peroxisome proliferator-activated receptor α-isoform deficiency leads to progressive dyslipidemia with sexually dimorphic obesity and steatosis. *J Biol Chem* 1998;273:29577–85.
20 Ip E, Farrell GC, Robertson G, *et al*. Central role of PPARalpha-dependent hepatic lipid turnover in dietary steatohepatitis in mice. *Hepatology* 2003;38:123–32.
21 Staels B, Rubenstrunk A, Noel B, *et al*. Hepatoprotective effects of the dual peroxisome proliferator-activated receptor alpha/delta agonist, GFT505, in rodent models of nonalcoholic fatty liver disease/nonalcoholic steatohepatitis. *Hepatology* 2013;58:1941–52.
22 Francque S, Verrijken A, Caron S, *et al*. PPARα gene expression correlates with severity and histological treatment response in patients with non-alcoholic steatohepatitis. *J Hepatol* 2015;63:164–73.
23 Liu S, Brown JD, Stanya KJ, *et al*. A diurnal serum lipid integrates hepatic lipogenesis and peripheral fatty acid use. *Nature* 2013;502:550–4.
24 Goto T, Lee JY, Teraminami A, *et al*. Activation of peroxisome proliferator-activated receptor-alpha stimulates both differentiation and fatty acid oxidation in adipocytes. *J Lipid Res* 2011;52:873–84.
25 Tsuchida A, Yamauchi T, Takekawa S, *et al*. Peroxisome proliferator-activated receptor (PPAR)α activation increases adiponectin receptors and reduces obesity-related inflammation in adipose tissue: comparison of activation of PPARα, PPARγ, and their combination. *Diabetes* 2005;54:3358–70.
26 Bünger M, van den Bosch HM, van der Meijde J, *et al*. Genome-wide analysis of PPARalpha activation in murine small intestine. *Physiol Genomics* 2007;30:192–204.
27 Sugden MC, Bulmer K, Gibbons GF, *et al*. Role of peroxisome proliferator-activated receptor-alpha in the mechanism underlying changes in renal pyruvate dehydrogenase kinase isoform 4 protein expression in starvation and after refeeding. *Arch Biochem Biophys* 2001;395:246–52.
28 Haemmerle G, Moustafa T, Woelkart G, *et al*. ATGL-mediated fat catabolism regulates cardiac mitochondrial function via PPAR-α and PGC-1. *Nat Med* 2011;17:1076–85.
29 Gentleman RC, Carey VJ, Bates DM, *et al*. Bioconductor: open software development for computational biology and bioinformatics. *Genome Biol* 2004;5:R80.
30 Fisher FM, Chui PC, Nasser IA, *et al*. Fibroblast growth factor 21 limits lipotoxicity by promoting hepatic fatty acid activation in mice on methionine and choline-deficient diets. *Gastroenterology* 2014;147:1073–83.e6.
31 Cotter DG, Ercal B, Huang X, *et al*. Ketogenesis prevents diet-induced fatty liver injury and hyperglycemia. *J Clin Invest* 2014;124:5175–90.
32 Hegardt FG. Transcriptional regulation of mitochondrial HMG-CoA synthase in the control of ketogenesis. *Biochimie* 1998;80:803–6.
33 Sahebkar A, Chew GT, Watts GF. New peroxisome proliferator-activated receptor agonists: potential treatments for atherogenic dyslipidemia and non-alcoholic fatty liver disease. *Expert Opin Pharmacother* 2014;15:493–503.
34 Chakravarthy MV, Lodhi IJ, Yin L, *et al*. Identification of a physiologically relevant endogenous ligand for PPARalpha in liver. *Cell* 2009;138:476–88.
35 Chakravarthy MV, Pan Z, Zhu Y, *et al*. "New" hepatic fat activates PPARalpha to maintain glucose, lipid, and cholesterol homeostasis. *Cell Metab* 2005;1:309–22.
36 Chen W, Zhou H, Liu S, *et al*. Altered lipid metabolism in residual white adipose tissues of Bscl2 deficient mice. *PLoS ONE* 2013;8:e82526.
37 Caspar-Bauguil S, Kolditz CI, Lefort C, *et al*. Fatty acids from fat cell lipolysis do not activate an inflammatory response but are stored as triacylglycerols in adipose tissue macrophages. *Diabetologia* 2015;58:2627–36.
38 Sanderson LM, Degenhardt T, Koppen A, *et al*. Peroxisome proliferator-activated receptor beta/delta (PPARbeta/delta) but not PPARalpha serves as a plasma free fatty acid sensor in liver. *Mol Cell Biol* 2009;29:6257–67.
39 Jha P, Claudel T, Baghdasaryan A, *et al*. Role of adipose triglyceride lipase (PNPLA2) in protection from hepatic inflammation in mouse models of steatohepatitis and endotoxemia. *Hepatology* 2014;59:858–69.
40 Ziouzenkova O, Perrey S, Asatryan L, *et al*. Lipolysis of triglyceride-rich lipoproteins generates PPAR ligands: evidence for an antiinflammatory role for lipoprotein lipase. *Proc Natl Acad Sci USA* 2003;100:2730–5.
41 Jo YS, Ryu D, Maida A, *et al*. Phosphorylation of the nuclear receptor corepressor 1 by protein kinase B switches its corepressor targets in the liver in mice. *Hepatology* 2015;62:1606–18.
42 Jaeger D, Schoiswohl G, Hofer P, *et al*. Fasting-induced G0/G1 switch gene 2 and FGF21 expression in the liver are under regulation of adipose tissue derived fatty acids. *J Hepatol* 2015;63:437–45.
43 Markan KR, Naber MC, Ameka MK, *et al*. Circulating FGF21 is liver derived and enhances glucose uptake during refeeding and overfeeding. *Diabetes* 2014;63:4057–63.
44 De Sousa-Coelho AL, Marrero PF, Haro D. Activating transcription factor 4-dependent induction of FGF21 during amino acid deprivation. *Biochem J* 2012;443:165–71.
45 Iizuka K, Takeda J, Horikawa Y. Glucose induces FGF21 mRNA expression through ChREBP activation in rat hepatocytes. *FEBS Lett* 2009;583:2882–6.
46 Kim H, Mendez R, Zheng Z, *et al*. Liver-enriched transcription factor CREBH interacts with peroxisome proliferator-activated receptor α to regulate metabolic hormone FGF21. *Endocrinology* 2014;155:769–82.
47 Lu P, Yan J, Liu K, *et al*. Activation of aryl hydrocarbon receptor dissociates fatty liver from insulin resistance by inducing fibroblast growth factor 21. *Hepatology* 2015;61:1908–19.
48 Uebanso T, Taketani Y, Yamamoto H, *et al*. Liver X receptor negatively regulates fibroblast growth factor 21 in the fatty liver induced by cholesterol-enriched diet. *J Nutr Biochem* 2012;23:785–90.
49 Tanaka N, Takahashi S, Fang ZZ, *et al*. Role of white adipose lipolysis in the development of NASH induced by methionine- and choline-deficient diet. *Biochim Biophys Acta* 2014;1841:1596–607.
50 Jha P, Knopf A, Koefeler H, *et al*. Role of adipose tissue in methionine-choline-deficient model of non-alcoholic steatohepatitis (NASH). *Biochim Biophys Acta* 2014;1842:959–70.

Supplementary File 1

Supplementary Methods & References

Generation of *floxed-Pparα* mice

The *floxed-Pparα* mouse strain was generated at the Mouse Clinical Institute (Illkirch, France). High-fidelity PCR amplification of genomic DNA was used to generate a 4.5-kb 5′ long arm, a 0.7-kb targeting arm including exon 4 (FA: floxed fragment), and a 3.2-kb 3′ long arm including exon 5, which were assembled in a vector containing a neomycin resistance cassette and loxP and Flippase Recognition Target (FRP) sites. This targeting vector was electroporated into P1 ES cells (MCI-129Sv/Pas background). Homologous recombination was verified by PCR and Southern blot analysis using a Neoprobe, a 5′ external probe (5′-AATGTTAGACAGGAATGGCAATGCC-3′; 5′-CTCTGTGTACAGCTGTCTTTTGAAC-3′), a 3′ external probe (5′-CTACTGCCCTTGGTACCTTGAAATG-3′; 5′-CCTACCGTCTTTGTTACCTTCTTGC-3′), and three genomic DNA digestions (one with NsiI for the 5′ insertion and two with HindIII or NdeI for the 3′ insertion). To remove the neocassette, one positive ES cell clone was electroporated with a Flipase-expressing plasmid. The resultant recombination was screened by PCR.

The derived ES cell clones were injected into C57BL/6J blastocysts to produce chimeric mice expressing the *floxed-Pparα* locus. Mice carrying the floxed allele were genotyped by PCR using HotStar Taq DNA Polymerase (5 U/µL, Qiagen) and forward (Ef; 5′-CTGTACTTTGTAGACATCTGAGAGGCG-3′) and reverse primers (Er; 5′-TAGGTACCGTGGACTCAGAGCTAG-3′ (figure 1 A). The amplification conditions were as follows: 15 min at 95°C; then 25 cycles of 94°C for 1 min, 65°C for 1 min, and 72°C for 1 min; and 72°C for 10 min. The wild-type and floxed alleles amplified 279-bp and 380-bp fragments, respectively. The obtained conditional knockout mouse strain was backcrossed with C57BL/6J.

Generation of *Pparα* hepatocyte-specific knockout (*Pparα*$^{hep-/-}$) animals

Pparα$^{hep-/-}$ animals were created at INRA's rodent facility (Toulouse, France) by mating the *floxed-Pparα* mouse strain with C57BL/6J *albumin-Cre* transgenic mice (gifted from Prof. Didier Trono, EPFL, Lausanne, Switzerland) to obtain *albumin-Cre*$^{+/-}$*Pparα*$^{flox/flox}$ mice, i.e.

Ppar$\alpha^{hep-/-}$ mice. *Ppar*α deletion was confirmed by PCR using HotStar Taq DNA Polymerase (5 U/µL, Qiagen) and a forward (Lf; 5′-AAAGCAGCCAGCTCTGTGTTGAGC-3′ and reverse primer (Er; 5′-TAGGTACCGTGGACTCAGAGCTAG-3′) (figure 1A). Amplification conditions were as follows: 95°C for 15 min; followed by 35 cycles of 94°C for 1 min, 65°C for 1 min, and 72°C for 1 min; and 72°C for 10 min. This reaction produced 450-bp, 915-bp, and 1070-bp fragments with exon 4 deletion, the wild-type allele, and the floxed allele, respectively. The albumin-Cre allele was detected by PCR using the following primers pairs: CreU (5′-AGGTGTAGAGAAGGCACTTAG-3′ and CreD (5′-CTAATCGCCATCTTCCAGCAGG-3′), and G2lox7F (5′-CCAATCCCTTGGTTCATGGTTGC-3′) and G2lox7R (5′-CGTAAGGCCCAAGGAAGTCCTGC-3′). *Albumin-Cre*$^{-/-}$ *floxed-Ppar*α (*Ppar*$\alpha^{hep+/+}$) littermates and wild-type C57BL/6J mice were used as controls.

PPARα-deficient C57BL/6J mice (*Ppar*$\alpha^{-/-}$) were bred at INRA's transgenic rodent facility. Age-matched C57BL/6J mice (provided by Charles River) were acclimated to local animal facility conditions prior to experiments. Mouse housing was temperature-controlled (at 22-24°C), with a 12-hour light/12-hour dark cycle. All studied mice were male and were fed a standard rodent diet (Safe 04 U8220G10R). Mice were killed at Zeitgeber time (ZT) 14 unless stated otherwise, with ZT0 being when the lights are turned on and ZT12 when lights are turned off.

DNA preparation for genotyping

DNA was extracted from tail tissue and stored at −20°C. Samples were mixed with 75 µL 25 mM NaOH, and 0.2 mM NA_2EDTA (pH 12), then incubated for 10 min at 95°C. Samples were next cooled on ice for 10 min, mixed, and neutralized with 75 µL 40 mM Tris-HCL (pH 5.0). After centrifugation (6 min; 14 000 rpm), 2.5 µL of supernatant was used for PCR with HotStar Taq Polymerase (5 U/µL, Qiagen) following the manufacturer's instructions.

In vivo experiments

Fenofibrate treatment

Fourteen-week-old wild-type C57BL/6J (WT), floxed wild-type (*Ppar*$\alpha^{hep+/+}$), *Ppar*$\alpha^{hep-/-}$, and *Ppar*$\alpha^{-/-}$ mice received the PPARα agonist fenofibrate (Sigma) (100 mg/kg/day) or vehicle (aqueous 3% gum Arabic) by gavage for 10 days (n=6 animals/genotype/treatment).

Fasting and Fasting–refeeding experiment

Eight-week-old WT, (*Ppar*$\alpha^{hep+/+}$), *Ppar*$\alpha^{hep-/-}$, and *Ppar*$\alpha^{-/-}$ mice were fed *ad libitum*, fasted for 24 hours from ZT14, or fasted for 24 hours from ZT14 and then re-fed for the next 24 hours with glucose in water (200 g/L; Sigma). All mice were killed at ZT14 (n=6 mice/genotype/experimental condition). Wild-type (C57BL6/J) and *Fgf21*$^{-/-}$ mice (12 month-old) were sacrificed either at the fasted state (a 24hour fast) or at the fed state at ZT14, (n=5 mice/genotype/experimental condition).

Circadian experiment

Eleven-week-old C57BL/6J mice were fed *ad libitum* or fasted from ZT0–ZT24. At ZT0, ZT4, ZT8, ZT12, ZT14, ZT16, ZT20, and ZT24, six mice from each condition were killed by cervical dislocation.

CL316243 activation of β3-adrenergic receptor

Four-month-old (WT) and *Ppar*$\alpha^{hep-/-}$ mice were fasted at ZT0; given CL316243 (3 mg/mL/kg; Sigma C5976) or vehicle (0.5% carboxymethyl cellulose in sterilized water; Fluka, 21900) at ZT6; and killed at ZT14.

Nutritional challenge with a methionine- and choline-deficient (MCD) diet

Eighteen-week-old WT, *Ppar*$\alpha^{hep-/-}$, and *Ppar*$\alpha^{-/-}$ mice were fed for two weeks with a MCD (A02082002B) or control diet (A02082003B) obtained from Research Diet. Mice were killed at ZT8 (n=6 animals/genotype/group).

Nutritional challenge with a High Fat Diet

Eighteen-week-old WT, *Ppar*$\alpha^{hep-/-}$, and *Ppar*$\alpha^{-/-}$ mice were fed for two weeks with a HFD (D12492) or control diet (D12450J) obtained from Research Diet. Mice were killed at ZT8 (n=6 animals/genotype/group).

Aging experiment

WT, *Ppar*$\alpha^{hep-/-}$ and *Ppar*$\alpha^{-/-}$ mice (n=12 each) were weighed weekly for 51 weeks. Mice were then killed at ZT14.

Adenoviral FGF21 expression

FGF21 adenovirus or control (Genecust) was delivered to mice (WT, *Ppar*$\alpha^{hep-/-}$, and *Ppar*$\alpha^{-/-}$) through retro-orbital injection (5.10^9 [pfu]/mouse). Four days later, mice were fasted for 24h and sacrificed at ZT14.

Blood and tissue samples

Prior to sacrifice, blood was collected from the submandibular vein with a lancet into EDTA-coated tubes (BD Microtainer, K2E tubes). Plasma was prepared by centrifugation (1500*g*, 10 min, 4°C) and stored at −80°C. Following euthanasia by cervical dislocation, organs were removed, weighed, dissected when necessary, and prepared for histological analysis, or snap-frozen in liquid nitrogen and stored at −80°C.

Liver neutral lipids analysis

Tissue samples were homogenized in methanol/5 mM EGTA (2:1, v/v), and then lipids (corresponding to an equivalent of 2 mg tissue) were extracted following the Bligh–Dyer method using chloroform/methanol/water (2.5:2.5:2.1, v/v/v), in the presence of the internal standards glyceryl trinonadecanoate, stigmasterol, and cholesteryl heptadecanoate (Sigma). TGs, free cholesterol, and cholesterol esters were analysed by gas-liquid chromatography using a Focus Thermo Electron system with a Zebron-1 Phenomenex fused-silica capillary column (5 m, 0.32-mm i.d., 0.50-mm film thickness). Oven temperature was programmed to increase from 200 to 350°C at 5°C/min, and the carrier gas was hydrogen (0.5 bar). The injector and the detector temperatures were 315°C and 345°C, respectively.

Liver fatty acid analysis

To measure total hepatic fatty acid methyl ester (FAME) molecular species, lipids corresponding to an equivalent of 1 mg of liver were extracted in the presence of glyceryl triheptadecanoate (0.5 µg) as an internal standard. The lipid extract was transmethylated with 1 ml of BF3 in methanol (14% solution; Sigma-Aldrich) and 1 ml of hexane for 60 minutes at 100°C and evaporated to dryness, and the FAMEs were extracted with hexane/water (2:1). The organic phase was evaporated to dryness and dissolved in 50 µl ethyl acetate. A sample (1 µl) of total FAME was analyzed by gas-liquid chromatography (Clarus 600 Perkin Elmer system, with Famewax RESTEK fused silica capillary columns, 30-m×0.32-mm i.d., 0.25-µm film thickness). Oven temperature was programmed from 110°C to 220°C at a rate of 2°C per minute, and the carrier gas was hydrogen (7.25 psi). The injector and the detector were at 225°C and 245°C, respectively.

Transcriptomic analysis

A model was fitted using the limma lmFit function (1), and correction for multiple testing was applied using False Discovery Rate (Benjamini et al. 1995). Probes with an adjusted p value ≤0.05 were considered differentially expressed between conditions. Hierarchical clustering was applied to samples and differentially expressed probes using Pearson's correlation coefficient as distance and Ward's criterion for agglomeration. Gene Ontology (GO) Biological Process enrichment was evaluated using a conditional hypergeometric test (GOstats package,(3)). Functional annotation clustering of GO Biological Process were performed using DAVID Bioinformatics Resources 6.7 ((4,5)). Gene-gene interaction network were predicted using "Search Tool for the Retrieval of Interacting Genes" ((6) String V10).

Supplementary references

(1) Wettenhall JM, Smyth GK. limmaGUI: a graphical user interface for linear modeling of microarray data. Bioinformatics. 2004, 12;20(18):3705-6.

(2) Benjamini Y, Hochberg Y. Controlling the False Discovery Rate: A practical and powerful Approach to multiple testing. Journal of the royal Statistical Society. Series B (methodological), Vol.57, No.1 (1995), 289-300.

(3) Falcon S, Gentleman R. Using GOstats to test gene lists for GO term association. Bioinformatics. 2007 Jan 15;23(2):257-8.

(4) Huang DW, Sherman BT, Lempicki RA. Systematic and integrative analysis of large gene lists using DAVID Bioinformatics Resources. Nature Protoc. 2009;4(1):44-57.

(5) Huang DW, Sherman BT, Lempicki RA. Bioinformatics enrichment tools: paths toward the comprehensive functional analysis of large gene lists. Nucleic Acids Res. 2009;37(1):1-13.

(6) Szklarczyk D, Franceschini A, Wyder S, Forslund K, Heller D, Huerta-Cepas J, Simonovic M, Roth A, Santos A, Tsafou KP, Kuhn M, Bork P, Jensen LJ, von Mering C. STRING v10: protein-protein interaction networks, integrated over the tree of life. Nucleic Acids Res. 2015 Jan;43(Database issue):D447-52. doi: 10.1093/nar/gku1003.

Supplementary File 2: Oligonucleotide sequences for real-time PCR

Gene	NCBI Refseq	Forward primer (5'-3')	Reverse primer (5'-3')
Acadl	NM_007381	AGAAGTTCATCCCCCAGATGAC	GGCGTTCGTTCTTACTCCTTGT
Acox1	NM_015729	CAGACCCTGAAGAAATCATGTGG	CAGGAACATGCCCAAGTGAAG
Cyp4a10	NM_010011	TCCAGCAGTTCCCATCACCT	TTGCTTCCCCAGAACCATCT
Cyp4a14	NM_007822	TCAGTCTATTTCTGGTGCTGTTC	GAGCTCCTTGTCCTTCAGATGGT
Fasn	NM_007988	AGTCAGCTATGAAGCAATTGTGGA	CACCCAGACGCCAGTGTTC
Fgf21	NM_020013	AAAGCCTCTAGGTTTCTTTGCCA	CCTCAGGATCAAAGTGAGGCG
Fsp27	NM_178373	AGGCCCTGTCGTGTTAGCAC	CATGATGCCTTTGCGAACCT
G6pd	NM_019468	GTGGGATCCTGAGGGAAGAGT	GATGGTGGGATAGATCTTCTTCTTG
Hmgcs2	NM_008256	TGCAGGAAACTTCGCTCACA	AAATAGACCTCCAGGGCAAGGA
Plin5	NM_025874	CGCTCCATGAGTCAAGCCA	CTCAGCTGCCAGGACTGCTA
Pparα	NM_011144	CCCTGTTTGTGGCTGCTATAATTT	GGGAAGAGGAAGGTGTCATCTG
Pparβ/δ	NM_011145	AAGTGGCCATGGGTGACG	TGGTCCAGCAGGGAGGAAG
Pparγ	NM_011146	CCACCAACTTCGGAATCAGCT	TTTGTGGATCCGGCAGTTAAGA
Scd1	NM_009127	CAGTGCCGCGCATCTCTAT	CAGCGGTACTCACTGGCAGA
Tbp	NM_013684	ACTTCGTGCAAGAAATGCTGAA	GCAGTTGTCCGTGGCTCTCT
Tnfα	NM_013693	TCCCCAAAGGGATGAGAAGTTC	GCGCTGGCTCAGCCACT
Vnn1	NM_011704	ATGAGGTTTATGCCTTTGGAGC	CCACAGGTGCGTAAATTGGTAG

Supplementary File 3

A - Functional annotation clustering GO (p-value < 0.01; DAVID Bioinformatics Resources 6.7) of the 99 Genes down-regulated in *Pparα*$^{hep-/-}$ mice compared to WT mice whatever the dietary status (fed, fasted, fasted-refed).

Functional categories	GO references	Number of genes
Mitochondrion	GO:0005739	24
Oxidation reduction	GO:0055114	13
Mitochondrial part	GO:0044429	11
Fatty acid metabolic process	GO:0006631	8
Endoplasmic reticulum	GO:0005783	8

B - Predicted gene-gene interaction network (Search Tool for the Retrieval of Interacting Genes / String V10) amongst genes down-regulated in *Pparα*$^{hep-/-}$ mice compared to WT mice whatever the dietary status (fed, fasted, fasted-refed).

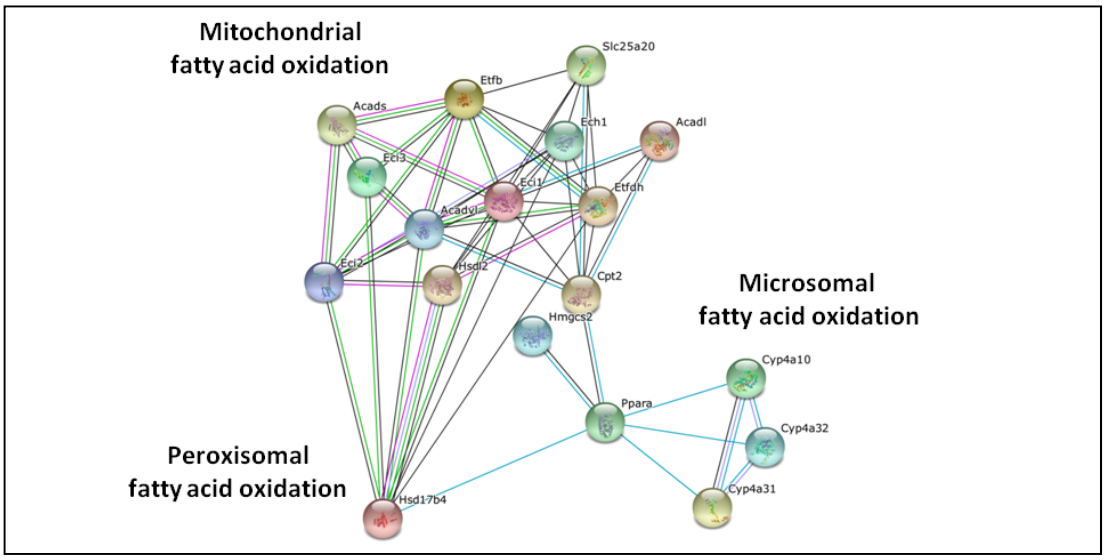

C - Functional annotation clustering GO (p-value < 0.01; DAVID Bioinformatics Resources 6.7) of the 27 Genes up-regulated in *Pparα*$^{hep-/-}$ mice compared to WT mice whatever the dietary status (fed, fasted, fasted-refed)

Functional categories	GO references	Number of genes
Endopeptidase activity	GO:0004175	4
Cytoskeleton organization	GO:0007010	3

Supplementary File 4

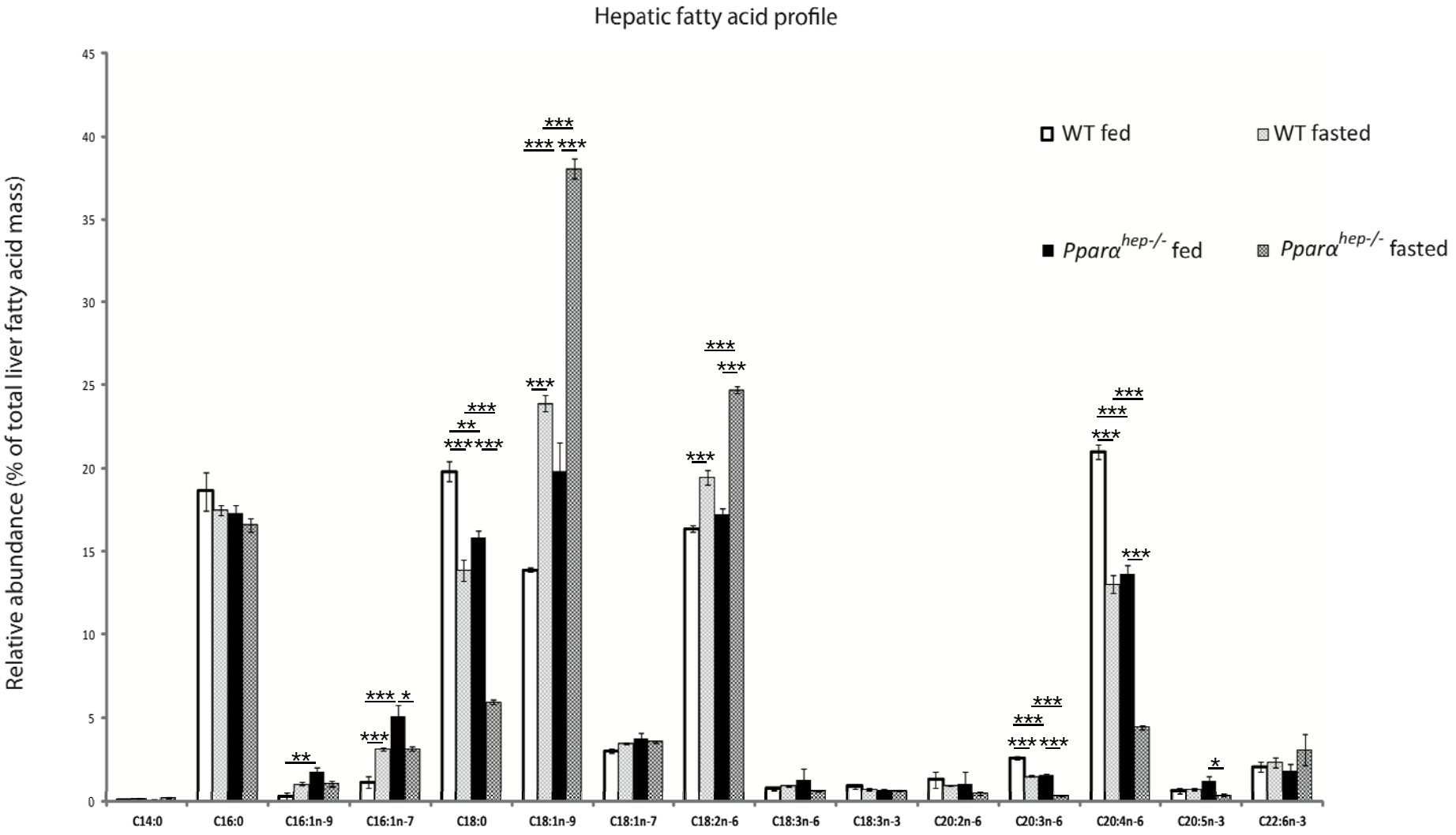

Hepatic fatty acid profile is modified by fasting and sensitive to hepatocyte *Pparα* deficiency. Relative abundance of hepatic fatty acids in WT and *Pparα*$^{hep-/-}$ mice fed or fasted for 24 hours was quantified by gas-liquid chromotography. Data are shown as mean ±SEM (n= 8 per group). *p≤0.05, **p≤0.01, ***p≤0.005.

(1) Gene Name	Regulation in fed mice over-expressing FGF21	(2)	Log FC $Ppar\alpha^{hep-/-}$ vs WT Fed	Adj.P. Val $Ppar\alpha^{hep-/-}$ vs WT Fed	Log FC $Ppar\alpha^{hep-/-}$ vs WT Fasted	Adj.P. Val $Ppar\alpha^{hep-/-}$ vs WT Fasted
Fmo	Up	*Fmo*	0,041	0,972	**1,909**	6,14E-06
Cyp2b9	Up	*Cyp2b9*	0,913	0,403	0,159	0,888
Mt1	Up	*Mt1*	**4,099**	3,34E-07	**1,110**	0,043
Igfal	Down	*Igfal*	0,076	0,942	-0,609	0,135
Ugt3a1	Down	*Ugt3a1*	**-2,070**	0,017	**-3,630**	1,08E-07
Osgin1	Down	*Osgin1*	-0,458	0,568	**1,162**	0,007
F11	Down	*F11*	0,229	0,520	**0,801**	5,52E-05
Scp2	Down	*Scp2*	0,085	0,632	-0,134	0,191
Aox3	Down	*Aox3*	**-1,032**	0,001	**-0,620**	0,014
Elovl3	Down	*Elovl3*	0,513	0,760	**-2,515**	0,001
Hes6	Down	*Hes6*	-0,087	0,860	-0,367	0,091
Selenbp2	Down	*Selenbp2*	ND	ND	ND	ND
Ela1	Down	*Ela1*	ND	ND	ND	ND
Ugt2b1	Down	*Ugt2b1*	-0,103	0,844	**0,881**	6,47E-05
Alas2	Down	*Alas2*	**0,586**	0,022	**0,418**	0,029
Nudt	Down	*Nudt*	-0,032	0,926	**-0,655**	1,18E-06
Gstp1	Down	*Gstp1*	-0,410	0,174	0,240	0,309
Cml4	Down	*Cml4*	ND	ND	ND	ND
Mcm10	Down	*Mcm10*	-0,842	0,149	-0,064	0,928
Sucnr1	Down	*Sucnr1*	**-2,181**	1,03E-05	**-1,792**	3,28E-06
C6	Down	*C6*	**0,254**	0,568	**0,927**	0,001
Cyp7b1	Down	*Cyp7b1*	0,418	0,515	-0,369	0,403
Cyp2d9	Down	*Cyp2d9*	-0,228	0,529	-0,373	0,077
Cyp4a12b	Down	*Cyp4a12b*	-0,461	0,466	**-1,277**	0,001
Mup4	Down	*Mup4*	0,095	0,627	-0,047	0,764
Serpina12	Down	*Serpina12*	**-1,947**	0,001	0,678	0,146
Serpina1e	Down	*Serpina1e*	**-0,565**	0,012	-0,149	0,490
Cyp4a12a	Down	*Cyp4a12a*	-0,663	0,248	**-1,303**	0,001
Hsd3b5	Down	*Hsd3b5*	-0,531	0,585	**1,377**	0,008

Up - regulated by FGF21 | Up - regulated by PPARα

Down - regulated by FGF21 | Down - regulated by PPARα

A: (1) Genes whose mRNA expression is significantly regulated in the liver of fed mice overexpressing FGF21 (data from GSE39313, Zhang *et al.*, 2012, Elife) and **(2)** their relative dependence on hepatocyte PPARα in our transcriptome analysis

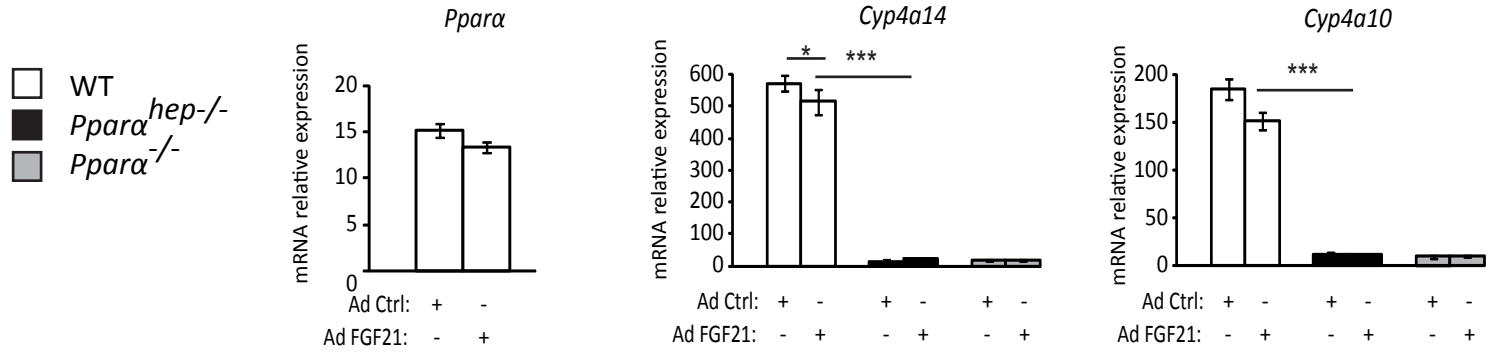

B: Hepatic mRNA expression levels of *Pparα*, *Cyp4a14* and *Cyp4a10* in response to 24h fasting with (+) or without (-) adenoviral overexpression of FGF21 in WT, $Ppar\alpha^{hep-/-}$ and $Ppar\alpha^{-/-}$ mice. Data are shown as mean ± SEM. *p≤0.05, **p≤0.01, ***p≤0.005.

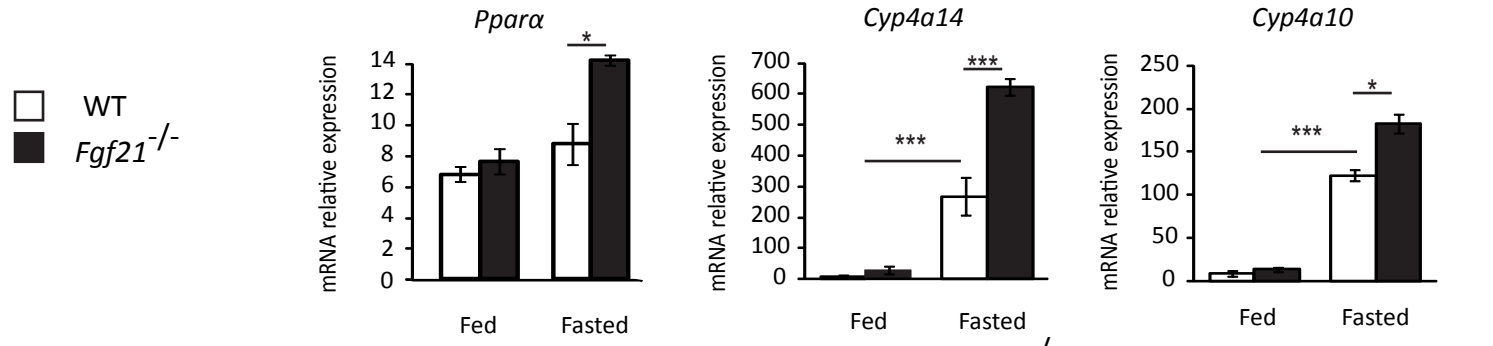

C: Hepatic mRNA expression levels of *Pparα*, *Cyp4a14* and *Cyp4a10* in WT and $Fgf21^{-/-}$ mice in response to 24h fasting. Data are shown as mean ± SEM. *p≤0.05, **p≤0.01, ***p≤0.005.

Supplementary File 6 **List of genes down-regulated by Fenofibrate (Log FC>1) and fasting in WT but not in PPARalpha hep-/-**

GeneName	SystematicName	logFC_LKO_Feno.LWT_Feno
Gm10804	NR_040533	4.338990155
Slco1a4	NM_030687	3.946688844
Gpr110	NM_133776	3.724069586
Blnk	NM_008528	3.594694282
Rgs16	NM_011267	3.328073207
Gck	NM_010292	2.704553909
Apoa4	NM_007468	2.698950403
Gm4477	NM_001253910	2.632084145
Ihh	NM_010544	2.628286186
Sdr9c7	NM_027301	2.600846197
Arhgef16	NM_001112744	2.600390221
Kcp	NM_001029985	2.587688912
Smpd3	NM_021491	2.502656144
Omd	NM_012050	2.446293066
Avpr1a	NM_016847	2.321034098
Clec2h	NM_053165	2.319711826
Cys1	NM_138686	2.251262731
Tuba8	NM_017379	2.21333475
Irf5	NM_012057	2.205714139
Il20	AK078698	2.188175561
Evc2	NM_145920	2.148281671
Il22ra1	NM_178257	2.14017001
Irx1	NM_010573	2.135892072
Plekhf1	NM_024413	2.071611419
Vasn	NM_139307	2.064549145

Cebpe	NM_207131	2.057939233
Cyp2c54	NM_206537	2.00580505
Fmn2	NM_019445	2.004180784
Ntf5	NM_198190	1.974077658
Espn	NM_207687	1.930187477
Usp18	NM_011909	1.929054274
Gldn	NM_177350	1.902430883
Snhg11	NM_175692	1.901885961
Gm10804	NR_040532	1.880303132
Mx2	NM_013606	1.833471447
Espn	NM_207687	1.752424815
Pkdcc	NM_134117	1.74787401
Dnajb11	NM_026400	1.693734168
Apol9a	NM_173786	1.682036041
Itpka	NM_146125	1.653329387
Evc	NM_021292	1.640295176
Cyp2c54	NM_206537	1.634821607
Ifi27l1	NM_026790	1.614340511
Nat8	NM_023455	1.611264421
Kalrn	ENSMUST00000023522	1.606828632
Sult1c2	NM_026935	1.597522687
Cyp2c50	NM_134144	1.530074931
Aqp4	NM_009700	1.520689629
Osgin1	NM_027950	1.51068762
Apol9b	NM_001168660	1.50682592
Apol9a	NM_173786	1.491777402
Cyp2c38	NM_010002	1.458490249
Plekhg5	NM_001004156	1.423607071

Rsad2	NM_021384	1.421197068
Irf7	NM_016850	1.419635985
Pde4b	NM_019840	1.416581869
Slco1a1	NM_013797	1.395577407
Slc17a1	NM_009198	1.37865757
Rtp4	NM_023386	1.36680329
Hist3h2a	NM_178218	1.361828009
Tnfrsf25	NM_033042	1.357712549
Cyp1a2	NM_009993	1.337789611
Synj2	NM_001113353	1.336116722
Kalrn	NM_177357	1.324905667
Slco2a1	NM_033314	1.323539871
Ifit1	NM_008331	1.320506833
Ear11	NM_053113	1.312705755
Crym	NM_016669	1.289927484
Nupr1	NM_019738	1.268707101
Tiam2	NM_011878	1.25324319
Gga2	NM_028758	1.248227354
Igsf8	NM_080419	1.245743645
Tmem161a	NM_145597	1.239198661
Pcp4l1	NM_025557	1.232257914
Hsd11b1	NM_008288	1.230227521
Samd1	NM_001081415	1.224727976
Dntt	NM_009345	1.21978365
Ppp4r4	NM_028980	1.213756156
Ugt2b1	NM_152811	1.209964061
Gstm2	NM_008183	1.205891998
C6	NM_016704	1.203122019

Gstm2	NM_008183	1.198638812
Pcbp4	NM_021567	1.189312741
Grm8	NM_008174	1.179630647
Gm2a	NM_010299	1.162405548
Pla1a	NM_134102	1.162394508
Ifit3	NM_010501	1.158512211
Gstm2	NM_008183	1.156968065
Oas1a	NM_145211	1.143199028
Oas1a	NM_145211	1.136708122
Lrp2	NM_001081088	1.123876743
Cdk20	NM_053180	1.115737794
Prodh	NM_011172	1.106241577
Mgat2	NM_146035	1.097829676
Cyp2c29	NM_007815	1.095120899
Mast4	NM_175171	1.091260632
Pcsk9	NM_153565	1.089930194
Adora1	NM_001008533	1.076713157
Gvin1	NM_029000	1.073977553
Pigf	NM_008838	1.069604813
Efhd2	NM_025994	1.062608113
Rtkn	NM_133641	1.061122385
Prss8	NM_133351	1.060518018
Armcx3	NM_027870	1.055236819
Oas1f	NM_145153	1.054884833
Slc37a1	NM_153062	1.05113534
Fam47e	NM_001033478	1.048260327
Wif1	NM_011915	1.047675224
Bhlhe40	NM_011498	1.041719532

Homer2	NM_011983	1.041124787
Mx1	NM_010846	1.039795857
Cmpk2	NM_020557	1.036328603
Agap2	NM_001033263	1.024070237
Prss8	NM_133351	1.020288658
Rnd2	NM_009708	1.017853772
Sqle	NM_009270	1.017528952
Neurl1a	NM_021360	1.009526359

Supplementary File 7: Functional annotation clustering GO (p-value < 0.01; DAVID Bioinformatics Resources 6.7) of the 698 Genes repressed by fenofibrate and fasting in WT and *Pparα hep+/+* but not in *Pparα hep-/-* mice (nor in *Pparα-/-* mice)

Functional categories	GO references	Number of genes
Endoplasmic reticulum	GO:0005783	61
Endoplasmic reticulum part	GO:0044432	24
Microsome	GO:0005792	13
Endosome	GO:0005768	21
Lysosome	GO:0005764	14
Regulation of Ras protein signal transduction	GO:0046578	13
Organic anion transmembrane transporter activity	GO:0008514	4

Supplementary File 8 **List of genes up-regulated by Fenofibrate (Log FC>2) and fasting in WT but not in PPARalpha hep-/-**

GeneName	SystematicName	logFC_LKO_Feno.LWT_Feno
Vnn1	NM_011704	-6.327507248
Cyp4a32	NM_001100181	-6.196767964
Cyp4a14	NM_007822	-5.960408744
Cyp4a31	NM_001252539	-5.634232845
Cyp4a10	NM_010011	-5.439267814
Krt23	NM_033373	-5.390005991
Cyp4a10	NM_010011	-5.344449564
Cyp4a10	NM_010011	-5.311799175
Rad51l1	NM_009014	-5.168389733
Gm15441	NR_040409	-5.022337513
Cyp4a31	NM_201640	-4.994452308
Agpat9	NM_172715	-4.981241516
Acot2	NM_134188	-4.774193064
Cyp4a31	NM_001252539	-4.739402899
Serinc2	NM_001253386	-4.694405198
Mfsd2a	NM_029662	-4.559186147
Rab30	NM_029494	-4.460954496
Serinc2	NM_172702	-4.442471841
Acot3	NM_134246	-4.39217577
Ehhadh	NM_023737	-3.943620325
Serinc2	NM_001253386	-3.720914131
Cidec	NM_178373	-3.699841322
Acot3	NM_134246	-3.695985114
Slc25a34	NM_001013780	-3.540701791

Tmem43	NM_028766	-3.519129781
Clstn3	NM_153508	-3.501309851
Dlg4	NM_007864	-3.459813265
Raet1e	NM_198193	-3.417569383
Acot5	NM_145444	-3.407106296
Rtn4	NM_194054	-3.319773259
Mtnr1a	NM_008639	-3.316641914
Gal3st1	NM_016922	-3.241994667
Mogat1	NM_026713	-3.208183376
Enc1	NM_007930	-3.202252717
Rufy4	NM_001034060	-3.201516745
Lgals4	NM_010706	-3.144456887
Spc25	NM_001199123	-3.115026503
Hsd17b11	NM_053262	-3.109470457
Lgals4	NM_010706	-3.092738086
Gm4952	NM_001013762	-3.043309935
Lgals4	NM_010706	-3.025184183
Fitm1	NM_026808	-3.02238903
Retsat	NM_026159	-2.986135359
Cda	NM_028176	-2.979215647
Qpct	NM_027455	-2.973192363
Gna15	NM_010304	-2.943823781
Cbfa2t3	NM_009824	-2.938950583
Fbf1	NM_172571	-2.901652108
Decr2	NM_011933	-2.836606019
Slc22a5	NM_011396	-2.815808723
Slc25a20	NM_020520	-2.793833675
G0s2	NM_008059	-2.791025291

Acaa1b	NM_146230	-2.786928971
Rab30	NM_029494	-2.77538891
Rarres1	NM_001164763	-2.7711581
Paqr7	NM_027995	-2.739895455
E2f8	NM_001013368	-2.739403931
Lgals6	NM_010707	-2.708925191
Tmtc2	NM_177368	-2.630701853
Slc35f2	NM_028060	-2.624275495
Ddhd2	NM_028102	-2.600504871
Cpt1b	NM_009948	-2.57618651
Nceh1	NM_178772	-2.551744536
Aldh3a2	NM_007437	-2.5462088
Abhd6	NM_025341	-2.541903604
Fitm2	ENSMUST00000109418	-2.541338387
Tmem98	NM_029537	-2.527726347
Plin5	NM_001077348	-2.522330477
Ech1	NM_016772	-2.510705785
Abhd6	NM_025341	-2.502624595
Paqr9	NM_198414	-2.492189808
Cox6b2	NM_183405	-2.488991428
Sema5b	NM_013661	-2.486591564
Chrna2	NM_144803	-2.443155692
Eci3	NM_026947	-2.432854016
Dnase1	NM_010061	-2.393569551
Sema5b	NM_013661	-2.389349368
Hr	NM_021877	-2.362630738
Etfdh	NM_025794	-2.361997894
Caln1	NM_021371	-2.338121081

Cerkl	NM_001048176	-2.325203282
Acsl1	NM_007981	-2.322008159
Tmed5	NM_028876	-2.320397015
Pex11a	NM_011068	-2.317353629
Acot8	NM_133240	-2.313631361
Eci2	NM_011868	-2.303602498
Slc6a16	XM_355900	-2.290913244
Slc22a21	NM_019723	-2.280482356
Unc5b	NM_029770	-2.270525456
Fitm2	NM_173397	-2.256975833
Cpt2	NM_009949	-2.250380721
Paqr9	NM_198414	-2.242478857
Cpt2	NM_009949	-2.23990941
Olfr15	NM_008762	-2.238433986
Raet1c	NM_009018	-2.222906132
Acot8	NM_133240	-2.218917378
Hsdl2	NM_024255	-2.216041134
Celf2	NM_010160	-2.210853201
Ctif	NM_201354	-2.180316331
Lamb3	NM_008484	-2.179424444
Mmd	ENSMUST00000004050	-2.168017347
Decr1	NM_026172	-2.167975542
Mmd	NM_026178	-2.16265343
Raet1b	NM_009017	-2.133017556
Celf2	NM_010160	-2.123555678
Crat	NM_007760	-2.116353216
Adam32	NM_153397	-2.08602317
Txnip	NM_001009935	-2.07753964

Pxmp4	NM_021534	-2.064830579
Slc16a11	NM_153081	-2.058554385
Slc16a13	NM_172371	-2.055575511
Mmd	ENSMUST00000134929	-2.022985304
Gm7969	XM_982175	-2.002981056

Supplementary File 9: Functional annotation clustering GO (p-value < 0.01; DAVID Bioinformatics Resources 6.7) of the 907 Genes induced by fenofibrate and fasting in WT and *Pparα hep+/+* but not in *Pparα hep-/-* mice (nor in *Pparα-/-* mice)

Functional categories	GO references	Number of genes
Mitochondrion	GO:0005739	219
Generation of precursor metabolites and energy	GO:0006091	50
Fatty acid metabolic process	GO:0006631	39
Peroxisome	GO:0005777	37
Mitochondrial matrix	GO:0005759	37
Cofactor binding	GO:0048037	37
Hydrogen ion transmembrane transporter activity	GO:0015078	17
Carboxylic acid catabolic process	GO:0046395	16
Cellular respiration	GO:0045333	16
O-acyltransferase activity	GO:0003988	11
Proteasome complex	GO:0000502	14
Nucleotide binding	GO:0000166	112
Iron ion binding	GO:0005506	26
Ligase activity, forming carbon-sulfur bonds,	GO:0016877	9
Oxidoreductase activity, acting on NADH or NADPH	GO:0016651	9
Acyl-CoA metabolic process	GO:0006637	7
Oxidative phosphorylation	GO:0006119	11
Cellular nitrogen compound biosynthetic process	GO:0044271	27
Protein homodimerization activity	GO:0042803	18
Vitamin metabolic process	GO:0006766	10
3-hydroxyacyl-CoA dehydrogenase activity	GO:0003857	5
Carboxylic acid binding	GO:0031406	12
Mitochondrial outer membrane	GO:0005741	10
Magnesium ion binding	GO:0000287	29
Oxidoreductase activity, acting on the CH-NH group of donors	GO:0016645	29
Mitochondrion organization	GO:0007005	13

A

GeneName	logFC fasted vs fed	adj.P.Val
Cyp4a14	*8.90*	*4.43E-20*
Cyp4a31	*6.45*	*2.71E-20*
Cyp4a10	*6.43*	*7.32E-20*
Igfbp1	6.04	6.91E-11
Cyp4a31	*5.56*	*5.01E-19*
Cyp4a32	*5.06*	*3.81E-14*
Apoa4	4.73	8.80E-17
Ppp1r3g	4.72	2.06E-08
Fsp27	*4.34*	*3.51E-14*
Acot3	*3.87*	*3.72E-11*
Fgf21	*3.86*	*1.14E-06*

B

GO_id	Term	Genes	p-value
GO:0006629	lipid metabolic process	26	2.01E-9
GO:0044281	small molecule metabolic process	31	2.14E-9
GO:0044710	single-organism metabolic process	47	5.03E-8
GO:0006082	organic acid metabolic process	22	2.14E-7
GO:0044699	single-organism process	84	3.45E-7
GO:0044763	single-organism cellular process	79	8.02E-7
GO:0019752	carboxylic acid metabolic process	20	1.68E-6
GO:0006790	sulfur compound metabolic process	13	2.27E-6
GO:0032787	monocarboxylic acid metabolic process	16	2.37E-6
GO:0043436	oxoacid metabolic process	20	6.9E-6
GO:0006637	acyl-CoA metabolic process	8	7.61E-6
GO:0035383	thioester metabolic process	8	7.61E-6
GO:0044255	cellular lipid metabolic process	19	8.09E-6
GO:0006732	coenzyme metabolic process	12	9.41E-6
GO:0001676	long-chain fatty acid metabolic process	8	2.29E-5
GO:0051186	cofactor metabolic process	12	1.09E-4
GO:0006631	fatty acid metabolic process	11	1.29E-3
GO:0032789	unsaturated monocarboxylic acid metabolic process	3	1.97E-3
GO:0032788	saturated monocarboxylic acid metabolic process	3	1.97E-3
GO:0032869	cellular response to insulin stimulus	8	3.62E-3
GO:0006641	triglyceride metabolic process	6	4.41E-3
GO:0008202	steroid metabolic process	9	8.25E-3
GO:0019217	regulation of fatty acid metabolic process	6	8.54E-3
GO:0006639	acylglycerol metabolic process	6	1.16E-2
GO:0006638	neutral lipid metabolic process	6	1.27E-2
GO:0009987	cellular process	79	2.97E-2
GO:0071375	cellular response to peptide hormone stimulus	8	4.35E-2
GO:0032868	response to insulin	8	4.75E-2
GO:0010565	regulation of cellular ketone metabolic process	7	6.67E-2
GO:1901653	cellular response to peptide	8	6.96E-2
GO:0008152	metabolic process	63	9.02E-2

C

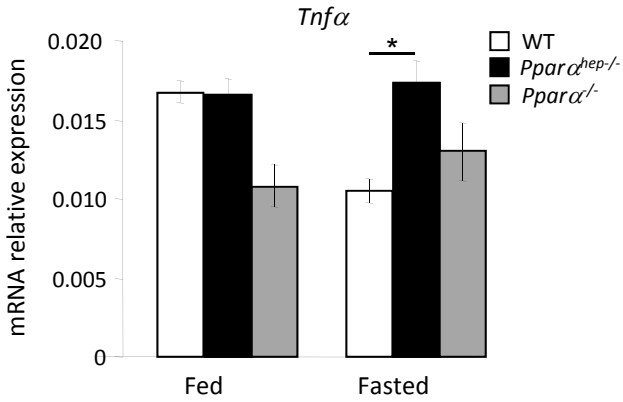

D

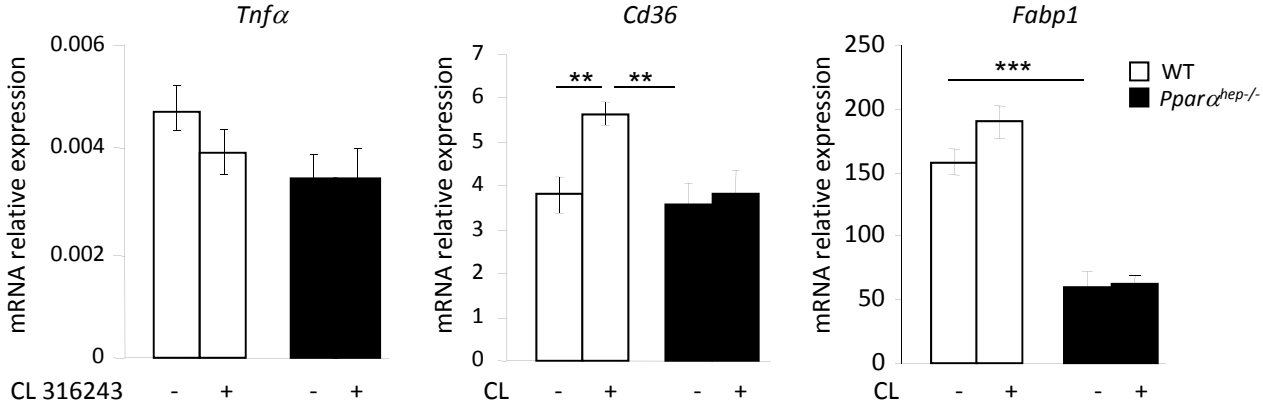

A. Top 11 genes induced by fasting in WT mice. In red genes regulated by fenofibrate and by fasting and dependent on hepatocyte PPARα activity. **B** Top GO biological process sensitive to fasting in WT mice (130 genes regulated with log FC>1.5). **C** Hepatic mRNA expression levels of *Tnfα* measured by qRT-PCR in liver samples of WT, *Pparα*$^{-/-}$, *Pparα*$^{hep-/-}$ 8 week-old male fed or fasted for 24 hours. **D**. Hepatic mRNA expression levels of *Tnfα*, *Cd36* and *Fabp1* measured by qRT-PCR in 4 month-old male WT and *Pparα*$^{hep-/-}$ mice treated with the β3-adrenergic receptor agonist CL316243 or vehicule at ZT6 and then killed at ZT14. Data are shown as mean ± SEM. *p≤0.05, **p≤0.01, ***p≤0.05.

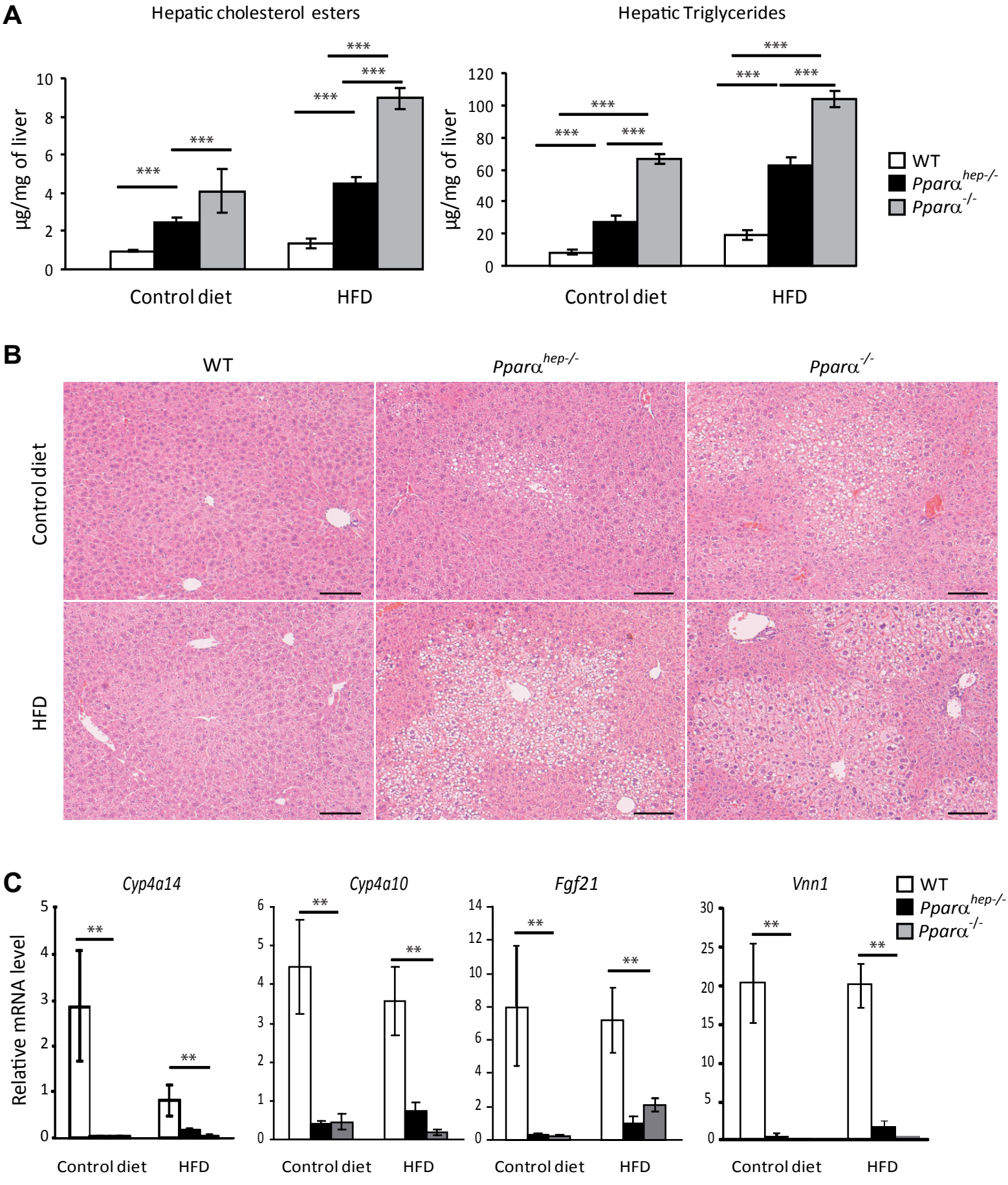

Liver PPARα deficiency aggravates steatosis in response to a High Fat Diet (HFD). Wild-type (WT), PPARα hepatocyte knockout (*Pparα*$^{hep-/-}$) and PPARα knockout (*Pparα*$^{-/-}$) mice were fed a HFD or a control diet for 2 weeks and were killed at ZT8. (A) Quantification of hepatic triglycerides and cholesterol esters. (B) Representative pictures of hematoxylin/eosin staining on liver sections. Scale bar, 100 µm. (C) Hepatic mRNA expression levels of *Cyp4a14, Cyp4a10, Fgf21* and *Vnn1*. Data are shown as mean +/- SEM. * p≤0.05, * p≤0.01, * p≤0.005.

A

Gene name	Ref Seq	Description	LogFC *Pparα* $^{hep-/-}$ vs WT	Adj.P.Val
Apon	NM_133996	Apolipoprotein N (Apon)	0.79	9.85E-05
Apof	NM_133997	apolipoprotein F (Apof)	0.37	0.016
Apol10a	NM_177744	Apolipoprotein L 10a	0.39	0.031
Apoa4	NM_007468	Apolipoprotein A-IV	1.97	6.03E-05
Abcg5	NM_031884	ATP-binding cassette, sub-family G (WHITE), member 5 (Abcg5)	-0.93	0.001
Abcg8	NM_026180	ATP-binding cassette, sub-family G (WHITE), member 8 (Abcg8)	-0.81	0.002
Abcb4	NM_008830	ATP-binding cassette, sub-family B (MDR/TAP), member 4 (Abcb4)	-0.53	0.009

B

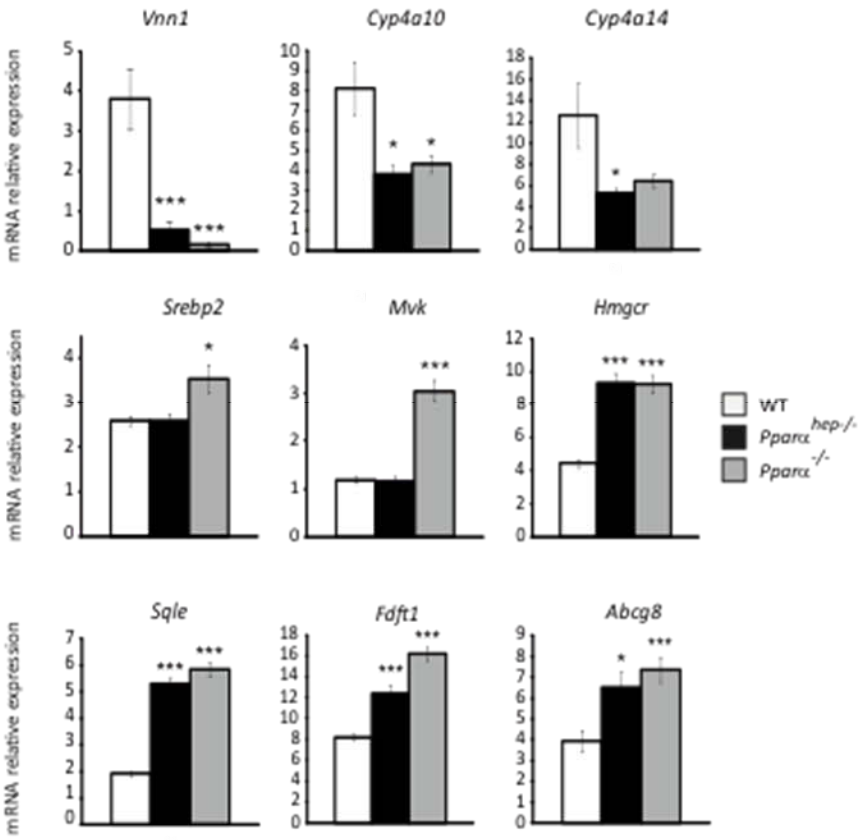

***Pparα* deficiency impact hepatic cholesterol metabolism.** A. Table listing significant differentially expressed genes related to cholesterol metabolism in liver samples from *Pparα*$^{hep-/-}$ vs WT mice. Data are extracted from microarrays analusis performed on samples from 8 week-old male mice in the fed state. B.Hepatic mRNA expression levels of PPARα target genes (*Vnn1*, *Cyp4a10* and *Cyp4a14*) and cholesterol metabolism related genes (*Srebp2*, *Mvk*, *Hmgcr*, *Sqle*, *Fdft1* and *Abcg8*) measured by qRT-PCR in fed 52 week-old male mice from WT, *Pparα*$^{hep-/-}$ and *Pparα*$^{-/-}$ genotypes. Data are shown as mean ± SEM. *p≤0.05, ***p≤0.005.